https://doi.org/10.5194/hess-2023-23
Preprint. Discussion started: 31 January 2023

Hydrology and Earth System Sciences
Discussions

Spatial distribution and controls of snowmelt runoff in a sublimation-dominated environment in the semiarid Andes of Chile

Álvaro Ayala[1], Simone Schauwecker[1], Shelley MacDonell[1, 2]

[1] Centro de Estudios Avanzados en Zonas Áridas (CEAZA), La Serena, 1700000, Chile
[2] Waterways Centre for Freshwater Management, Lincoln University and the University of Canterbury, Christchurch, New Zealand

Correspondence to: Álvaro Ayala (alvaro.ayala@ceaza.cl)

Abstract. Sublimation is the main ablation component of snow and ice in the upper areas of the semiarid Andes (~26-32°S and ~69-71°W). This region reaches up to 6000 m, is characterized by scarce precipitation, high solar radiation receipt, and low air humidity, and has been affected since 2010 by a severe drought. In this study, we suggest that most of the snowmelt runoff originates from specific areas with topographic and meteorological features that permit large snow accumulation and sufficient energy for snowmelt. We quantify the spatial distribution of snowmelt runoff and sublimation in a catchment of the semiarid Andes using a process-based snow model that is forced and validated with field data, satellite-derived indices of snow presence and an independent SWE reconstruction product. Results from model simulations over a two-year period reproduce point-scale records of snow depth and SWE and are also in good agreement with distributed patterns obtained from satellite-derived products, such as snow cover area and indices of snow absence and persistence. We estimate that 50% of snowmelt runoff is produced by 18-28% of the catchment area, which we define as "snowmelt hotspots". Snowmelt hotspots are located at elevations between 4200 and 4800 m, have easterly aspects, low slope angles, and high snow accumulation and persistence. We suggest that snowmelt hotspots play a key hydrological role when connecting with other features of dry mountain regions, such as areas of groundwater recharge, rock glaciers and mountain peatlands, and recommend more detailed snow and hydrological monitoring of these sites, especially in the current and projected scenarios of scarce precipitation.

https://doi.org/10.5194/hess-2023-23
Preprint. Discussion started: 31 January 2023


Hydrology and Earth System Sciences
Discussions

1 Introduction

Snowmelt is typically the largest runoff contributor in high-elevation mountain regions and their adjacent areas (Mankin et al., 2015; Kraaijenbrink et al., 2021). The annual volume of snowmelt runoff generated from each catchment is the result of the interactions between the topography, the land cover and the physical processes that control snowfall, snow transport, the surface energy balance and the internal changes of the snowpack (Lehning et al., 2008; Mott et al., 2018; Pomeroy et al., 1998). A good understanding of these processes and how to model them is key to quantify water supply availability for several populated regions around the world (Freudiger et al., 2017; Hock et al., 2017). A particularly critical case of snowmelt dependency is that of arid and semiarid high-elevation mountain ranges, such as the semiarid Andes, Central Asia, and Southwestern USA (Huning and AghaKouchak, 2020). The climate of these mountain ranges is characterized by low temperatures and little precipitation (hereafter we refer to these ranges as cold and dry mountain regions), and pose characteristic challenges to estimate snowmelt runoff, such as episodic precipitation events (Schauwecker et al., 2022), shallow snowpacks (Zhang and Ishikawa, 2008) and high sublimation rates (Stigter et al., 2018).

Sublimation from the snow cover is the direct transition of water from solid to vapor state and it occurs as surface sublimation (e.g. Hood et al., 1999), or as blowing (or drifting) snow sublimation (e.g. Groot Zwaaftink et al., 2013). Both surface and blowing snow sublimation reduces the mass of the snow cover and can significantly affect the water balance of various regions around the world, such as the Canadian Prairies (Pomeroy and Li, 2000), Antarctica (Palm et al., 2017), and the semiarid Andes (Réveillet et al., 2020; Gascoin et al., 2013). Additionally, turbulent latent heat fluxes associated with the solid to vapor transition lowers the temperature of the snow surface, thus decreasing the energy available for melting. This process can have impacts on glacier mass balance (Ayala et al., 2017a; Stigter et al., 2018) and the performance of temperature-index melt models (Ayala et al., 2017b; Litt et al., 2019). Blowing snow sublimation depends on the amount of transported snow and sublimation rates and is usually important in the mass balance of open and windswept environments (Pomeroy and Li, 2000), and wind-exposed mountain ridges (Strasser et al., 2008).

Both snowmelt and surface sublimation are determined by the surface energy balance of the snow cover. The spatial variability of the energy balance can be very large and is controlled by snow accumulation, solar radiation and snow-atmosphere interactions that evolve during the ablation season (Mott et al., 2018; Pomeroy et al., 2003). By the end of the ablation season, snow cover often reaches a patchy state in which the advection of sensible and latent heat from snow-free areas play a key role for snow and ice ablation (Mott et al., 2020; van der Valk et al., 2022). Solving the energy balance of the snow cover over complex and steep terrain is a very complex task, as it depends on the availability of distributed meteorological forcing data and adequate parameterizations of the physical processes controlling radiation, turbulent fluxes, snow microstructure and snow metamorphism (Vionnet et al., 2012; Lehning et al., 2002). Despite this complexity, in hydrological models the temporal and spatial variability of the energy balance is usually averaged over elevation bands or other hydrological units, but with negative effects on the representation of snow ablation and runoff at the basin scale (Dornes et al., 2008; Luce et al., 1998). In cold and dry mountain regions, turbulent latent heat fluxes and sublimation can represent a large part of the snow cover energy and

https://doi.org/10.5194/hess-2023-23
Preprint. Discussion started: 31 January 2023


Hydrology and Earth System Sciences
Discussions

mass balance (Jackson and Prowse, 2009; Zhang and Ishikawa, 2008), suggesting a particularly large spatial variability of snowmelt and runoff generation. However, snow sublimation is frequently neglected in hydrological models (e.g. Ragettli et al., 2014; Seibert et al., 2017).

The semiarid Andes is a good example of a snowmelt-dependent region where snow sublimation can significantly reduce the mass of the winter snow cover and complicate the calculation of snowmelt runoff. Several studies have estimated snow mass and energy balances (Gascoin et al., 2013; Réveillet et al., 2020; Voordendag et al., 2021), and have provided useful insights into processes occurring in this region, as well as into the challenges of estimating distributed snowmelt and sublimation in this environment. However, these studies have largely focused on either model or input uncertainties (Réveillet et al., 2020; Voordendag et al., 2021), or snow redistribution (Gascoin et al., 2013), rather than hydrological importance. From another perspective, Mendoza et al. (2020) analyzed the strong relation between snow depth and local topographic and land cover properties in semiarid catchments of central Chile. Given that snow represents 85% of streamflow variability in semiarid catchments (Masiokas et al., 2006) and is a useful predictor of streamflow (Sproles et al., 2016), it is of vital importance to connect distributed snow mass and energy balance processes to hydrological impacts in their full complexity and spatial variability.

In this work, we hypothesize that the meteorological and topographical conditions of the semiarid Andes result in large areas where snow surface sublimation losses dominate over snowmelt, thus delimiting relatively small areas from where most of the catchment runoff is generated. We refer to these sites as “snowmelt hotspots” and we define them as those forming the minimum area in a snow-covered catchment from where at least 50% of the snowmelt runoff is generated. To test this hypothesis, we calculate spatially distributed amounts of snowmelt and snow sublimation using a process-based snow evolution model in a 79 km^2 catchment of the semiarid Andes of Chile over a two-year period (April 2019 to March 2021). The model is forced with in-situ meteorological data, and it is verified against point observations of snow variables and remote sensing products. Our main objectives are to i) quantify the snow mass balance components, ii) determine the existence and location of snowmelt hotspots, and iii) identify the main characteristics of the snowmelt hotspots. We expect that our results will provide new insights for studies focusing on snowmelt runoff generation in cold and dry mountain regions and its connection with other components and processes, such as glaciers, permafrost, groundwater recharge and the spatial distribution of vegetation.

2 Study area

The semiarid Andes of Chile extend from approximately 26°S to 32°S (~69-71°W) reaching elevations up to more than 6000 m a.s.l. Its climate is defined as cold semi-arid with dry summers in the low-lying areas up to approximately 3000 m a.s.l. and as tundra climate in the upper areas (Sarricolea et al., 2017). While winters are cold with occasional precipitation events, summers are hot and dry with low cloudiness and intense solar radiation (Favier et al., 2009). Precipitation has a large interannual variability mostly associated with El Niño Southern Oscillation (ENSO) (Arias et al., 2021; Montecinos and

https://doi.org/10.5194/hess-2023-23
Preprint. Discussion started: 31 January 2023

Aceituno, 2003). Annual precipitation in the lowlands increases from ca. 100 to 300 mm a^{-1} towards south and is 3-5 times higher near the peak of the Andes, but it usually does not increase significantly above 3000 m.a.sl. (Scaff et al., 2017; Favier et al., 2009). Cloud cover and air moisture are usually very low, which determines very high values of solar radiation and potential evapotranspiration (MacDonell et al., 2013). Snowmelt is the main runoff contributor in this region, even though mass losses produced by snow sublimation can reach up to 50 or 80% of the annual snowfall (Réveillet et al., 2020). Glacier runoff is also an important contributor during droughts and at the end of summer (Gascoin et al., 2011; Ragettli et al., 2014).

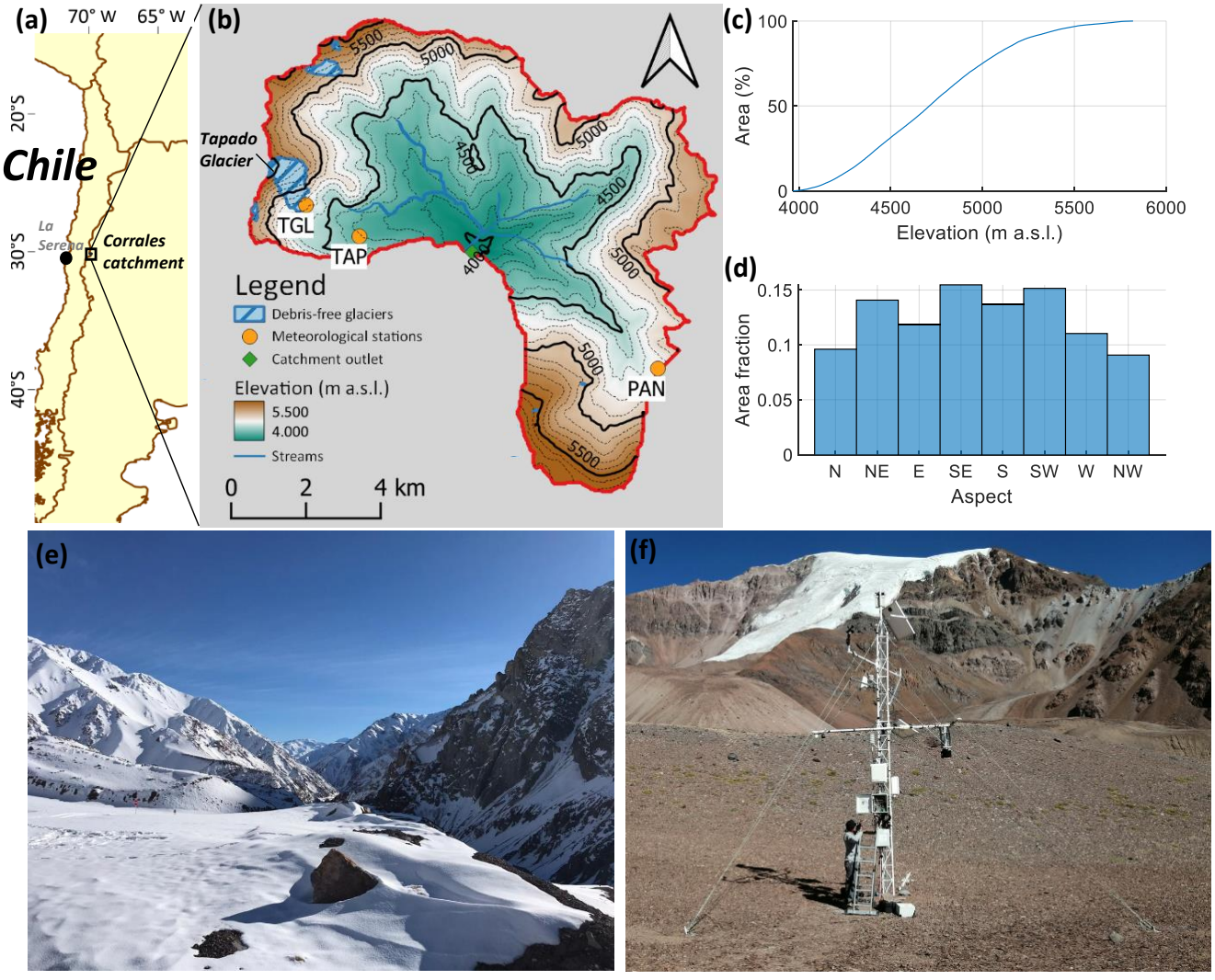

Figure 1: (a): Location of the Corrales catchment in Chile, (b) Map of the Corrales catchment including Tapado Glacier and the Tapado (TAP), Tapado Glacier (TGL) and Paso Agua Negra (PAN) meteorological stations, (c) Hypsometry of the basin, (d) Slope aspect frequency distribution in the catchment, (e) Winter snow accumulation close to La Laguna reservoir (~3200 m a.s.l.), (f) Tapado AWS with Tapado Glacier in the background.

https://doi.org/10.5194/hess-2023-23
Preprint. Discussion started: 31 January 2023


Hydrology and Earth System Sciences Discussions

This study focuses on the Corrales catchment, a 79 km^2 catchment (30.16°S, 69.88°W) located in the upper areas of the semiarid Andes of Chile, approximately 180 km east of La Serena city (Figure 1a-b). The elevation of the catchment ranges from 3800 to 5600 m a.s.l., with ca. 50% of the catchment located above 4700 m a.s.l. (Figure 1c). The orientation of the slopes is relatively uniform across the catchment (Figure 1d). Meteorological records from the nearby La Laguna meteorological station (30.20°S, 70.04°W, 3160 m a.s.l., maintained by the Chilean Water Directorate (DGA)) show an annual mean precipitation of 160 mm a^{-1} (with a coefficient of variation of 0.68) and an average temperature of 8.1ºC in the period 1965-2020. Snow varies spatially across the catchment (Figure 1e), and resultant runoff leaving the Corrales catchment is stored in La Laguna Reservoir (40 Mm^3) from where it is regulated for irrigation and other uses. Above 3000 m a.s.l. vegetation is almost completely absent except for peatlands next to streams (Valois et al., 2020) and shrubs on the mountain slopes (Kalthoff et al., 2006). Corrales catchment contains Tapado Glacier, which is the largest glacier on the Chilean side of this region (1.67 km^2 in 2019) (DGA, 2022). Tapado Glacier has lost 25.2 ± 4.6% of its area since 1956, with an accelerated negative mass balance since 2000 (Robson et al., 2022), which is in line with other glaciers in the area (Pitte et al., 2022). In addition, the Corrales catchment contains a few small debris-free glaciers located above 5000 m a.sl. (Figure 1b), and several rock glaciers that might play a relevant hydrological role (not shown) (Schaffer et al., 2019). Since 2009, the Corrales catchment has been instrumented with hydrometeorological equipment and several field campaigns have been carried out, focusing on the collection of groundwater, glaciological and hydrological data (e.g., Figure 1f).

3 Data

3.1 Field data

We use meteorological data from a network of stations in the Corrales basin to force a snow evolution model that is presented in Section 4. The meteorological network consists of three AWSs: Tapado (TAP), Tapado Glacier (TGL) and Paso Agua Negra (PAN) (Figure 1 and Table 1). The AWSs are maintained by the Centro de Estudios Avanzados en Zonas Áridas (CEAZA), based in La Serena, Chile, and are visited several times each year between October and May when the site is accessible by road. TAP and PAN consist of meteorological towers (Figure 1f, S1a) and transmit near-real time data via satellite communication. TGL is a HOBO U30 station installed on a tripod next to the lower debris-free section of Tapado Glacier that is visited with a lower frequency (2 to 3 times per year) due to logistical limitations (Figure S1b). Data from TGL is downloaded manually.

Hourly precipitation is derived from the cumulative precipitation data recorded at TAP (Table 1). As the cumulative precipitation record contains noise, we apply a simple method that discriminates actual precipitation from sensor noise (see Section S1). Additionally, based on a comparison with the SWE sensor and results from previous studies at TAP (Réveillet et al., 2020; Voordendag et al., 2021), we increase precipitation amounts by 30% due to snow undercatch by the sensor and precipitation underestimation due to differences between the exact location of the precipitation sensor and the meteorological tower where snow depth and SWE are recorded. Following these corrections, we obtain total precipitation amounts of 309 mm

https://doi.org/10.5194/hess-2023-23
Preprint. Discussion started: 31 January 2023


Hydrology and Earth System Sciences
Discussions

and 330 mm in the hydrological years 2019-2021 and 2020-2021 (from April to March), respectively (Figure 2a). Although annual precipitation was higher in 2020-2021, precipitation in the main snow season (April-September) was higher in 2019 (238 mm compared with 196 mm). Although we do not have a long-term precipitation at this particular site, we verified that, according to La Laguna DGA precipitation records (Información Oficial Hidrometeorológica y de Calidad de Aguas en Línea, 2023), our study years (2019-2020 and 2020-2021) corresponded to a dry period, with an annual exceedance probability of ca. 80% for both years.

Figure 2 shows a summary of the data collected by the three AWSs during the study period and Table 1 includes more details, such as the sensors and their installation heights. Apart from occasional gaps at each station, the largest period of missing data is found at TAP between December 2020 and January 2021. Daily mean air temperature at the elevation of TAP remained above 0°C for several months (November to April), with a maximum near 10°C in January 2020 (Figure 2a), although there was a large data gap in summer 2021. Since the correlation between the three air temperature records is very high ($R^2 > 0.95$), missing data was filled by establishing linear relationships between the three stations. Figure 2b shows the variability of snow depth, SWE and surface albedo at TAP. Snow depth reached up to 1 m in the winter 2019, but only 0.8 m in the winter 2020. In general, snow depth decreases rapidly during the days following each snowfall event. SWE and surface albedo closely followed snow depth variations. We found that the decay of surface albedo was faster in spring 2019 than in 2020. Mean daily solar radiation reached values up to more than 400 W m^{-2} with frequent drops associated with cloudiness, especially in the winter period (Figure 2c). The seasonal variability of incoming longwave radiation was much lower than that of solar radiation and varies between 180 and 300 W m^{-2} (Figure 2c). Daily mean relative humidity at TAP remained mostly below 50% for most of the time, increasing above this value only a few times during the study period (Figure 2d). Relative humidity at the other stations was similar (not shown). Air pressure varied between 550 and 580 hPa with large and relatively constant values in summer and low and oscillating values in winter (Figure 2d). Wind speed at PAN was 2.6 times larger than at TAP and TGL, with a large predominance of western winds, indicating that the latter are located at wind-sheltered locations (Figure 2e and 2f).

In addition to the meteorological data, we use a dataset of surface elevation changes of Tapado Glacier to validate ice melt estimates produced by the snow evolution model (Section 4). These observations correspond to ablation stake readings collected in the summer periods 2019-2020 and 2020-2021, and snow density measurements at the end of the corresponding spring periods. The stakes were manually drilled on the ablation zone of the glacier and were visited approximately every month during the ablation season (Figure S2 and Table S1). The visit and maintenance of the ablation stakes was difficult due to the development of snow and ice penitentes of 3-4 m height (Figure S3), which also led to the collapse of some monitored sites. Penitentes are cone-shaped snow and ice structures formed in dry environments by differential ablation rates along their height (Lliboutry, 1954). The ablation stakes network consists of traditional single-point measurements and one 5-m ablation transect where we registered surface lowering every 20 cm to account for the differential ablation of the surface associated with the penitentes following Nicholson et al. (2016).

https://doi.org/10.5194/hess-2023-23
Preprint. Discussion started: 31 January 2023


Hydrology and Earth System Sciences
Discussions

Table 1: AWSs in the Corrales catchment

Station	Name	East	South	Elevation	Monitored variables (*)	Instrument	Sensor height (m)
TAP	Tapado	412546	6663325	4306	T-RH	Vaisala HMP45C	4.0
					WS-WD	RM Young 5103 Wind Monitor	5.0
					P	Geonor T-200B 1000 mm	1.5
					Sin-Sout-Lin	Kipp and Zonen CNR4	3.5
					SD	Luft SHM31	3.5
					SWE	Campbell CS725	3.0
TGL	Tapado Glacier	411121	6664158	4727	T-RH	HOBO S-THB-M002	2.0
					WS	HOBO S-WSA-M003	2.0
					WD	HOBO S-WDA-M003	2.0
					Sin-Sout	HOBO S-LIB M003	2.0
PAN	Paso Agua Negra	420534	6659795	4774	T-RH	Vaisala HMP155	3.0
					WS-WD	Campbell CSAT3	5.0
					Pa	Vaisala PTB110	2.0

(*): T: Air temperature, RH: Relative humidity, WS: Wind speed, WD: Wind direction, P: Precipitation, Sin: Incoming solar radiation, Sout: Reflected solar radiation, Lin: Incoming longwave radiation, SD: Snow depth, SWE: Snow water equivalent, Pa: Air pressure.

https://doi.org/10.5194/hess-2023-23
Preprint. Discussion started: 31 January 2023

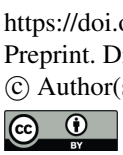

Hydrology and Earth System Sciences
Discussions
Open Access
EGU

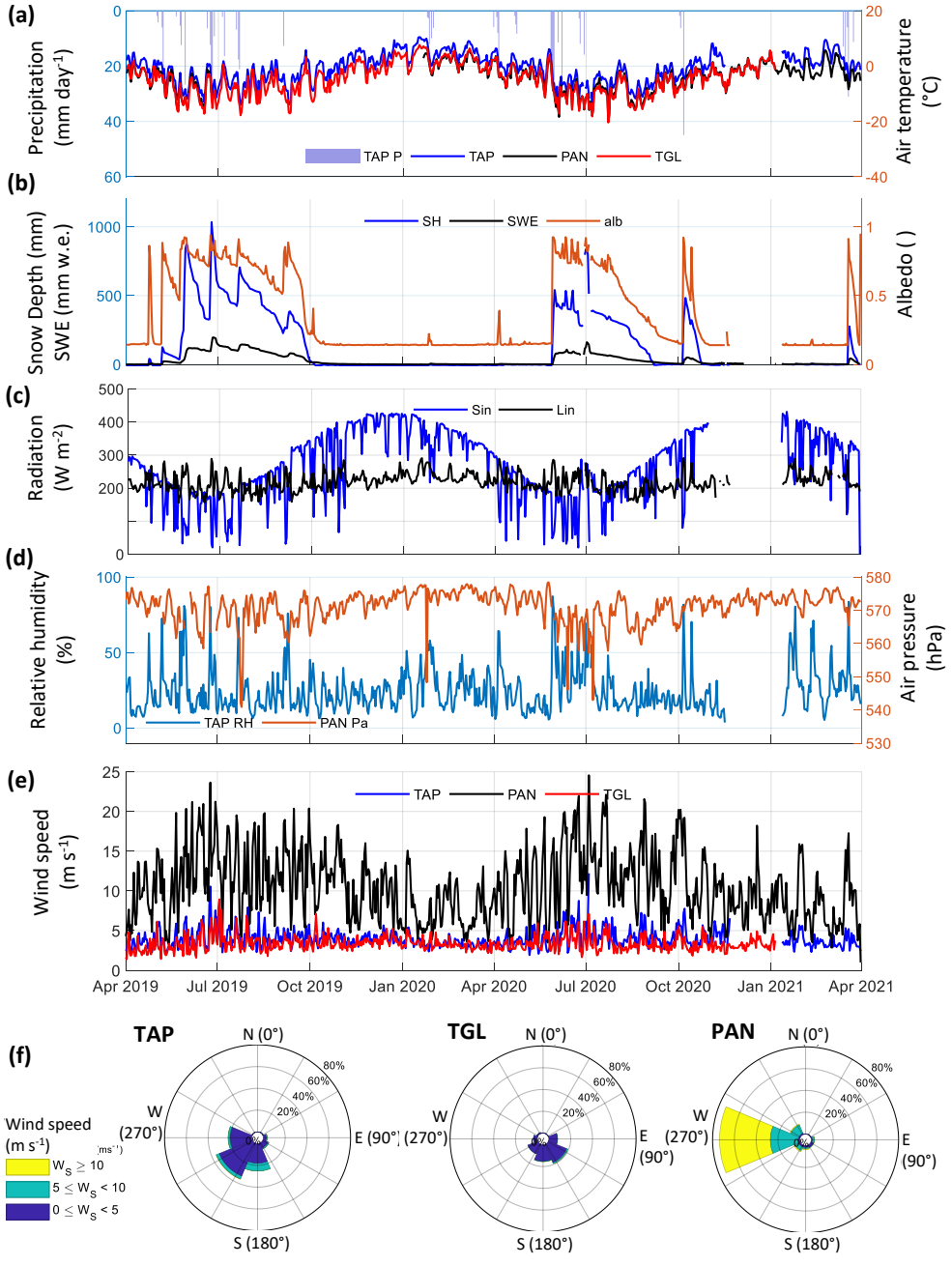

Figure 2: Meteorological time series recorded at Tapado (TAP), Tapado Glacier (TGL) and Paso Agua Negra (PAN) during the study period. If not indicated, the meteorological variables were recorded at TAP. (a) Precipitation (left axis) and air temperature (right axis), (b) Snow depth, SWE, and albedo, (c) Incoming shortwave and longwave radiation, (d) Relative humidity and air pressure, (e) Wind speed, (f) Wind roses.

https://doi.org/10.5194/hess-2023-23
Preprint. Discussion started: 31 January 2023


Hydrology and Earth System Sciences
Discussions

3.2 Snow products

We use two spatially distributed datasets that describe the interannual and seasonal variations of the snow cover to evaluate the results of the snow evolution model (Section 4). The first dataset corresponds to satellite-based maps of snow absence and persistence indices (Wayand et al., 2018) in the period 2019-2021, the second to SWE daily maps that were reconstructed using a data assimilation scheme for the subtropical Andes in the period 1985-2015 (Cortés and Margulis, 2017).

3.2.1 Maps of snow absence (SA) and snow persistence (SP) indices

We use the snow indices defined by Wayand et al. (2018) to characterize the spatial patterns of snow cover in the study area. The snow absence (SA) index is defined as the fraction of time in which snow is absent during the accumulation period, whereas the snow persistence (SP) index is defined as the fraction of time in which snow is present during the melt period. In their study, Wayand et al. (2018) developed a method to estimate SA and SP from optical satellite images obtained by Sentinel-2 and Landsat-8 missions. The method was implemented in the Google Earth Engine platform, which is freely available. In our study, we adapt the definition of the snow accumulation and melt periods to the Southern Hemisphere (accumulation: April-September and melt: October-March) and apply the method to the Corrales catchment. A summary of the utilized images is given in Table 2 (see Table S2 for the full list of images).

Table 2: Summary of satellite images used for the calculation of the snow indices (SA and SP)

Snow index	Months	Product	Period	Number of images
Snow absence	April to September	Landsat-8	13-04-2019 to 22-09-2020	18
		Sentinel-2	03-06-2019 to 10-09-2020	15
Snow persistence	October to March	Landsat-8	06-10-2019 to 17-03-2021	21
		Sentinel-2	15-11-2019 to 14-03-2021	23

3.2.2 Maps of reconstructed SWE

We analyze the spatial variability of snow accumulation in the study area using the SWE reconstruction developed by Cortés and Margulis (2017). This dataset consists of daily maps of SWE with a spatial resolution of 180 m over the extratropical Andes (27-37°S) in the period 1985-2015. The maps were calculated using a data assimilation scheme that combines results from a Land Surface Model and Landsat optical images. The data assimilation scheme explicitly addresses the uncertainty of input variables by weighting simulation ensembles to fit observed fractional snow cover area (SCA) from the satellite images. Reconstructed SWE maps compare well with manual records along the Andes (Cortés and Margulis, 2017; Cortés et al., 2016) and melt season runoff records (Alvarez-Garreton et al., 2018). Later results have shown that these maps are suitable for other analyses, such as the impact of atmospheric rivers on snow accumulation (Saavedra et al., 2020) and the validation of hydrological models (Ayala et al., 2020).

https://doi.org/10.5194/hess-2023-23
Preprint. Discussion started: 31 January 2023


Hydrology and Earth System Sciences
Discussions

3.3 Other data

Catchment topography is extracted from a ~30 m resolution Digital Elevation Model (DEM) produced by NASADEM (NASA JPL, 2020). Additionally, we use the Normalized Difference Snow Index (NDSI) derived by the Sentinel-2 Level 2A processing (Level-2A Algorithm Overview, 2023) to calculate SCA over the study catchment and compare it with our model simulations (see section 4). We manually selected a total of 103 cloud-free NDSI maps in the period April 2019-March 2021 using the EO Browser (https://apps.sentinel-hub.com/eo-browser/).

4 SnowModel

4.1 Model description

SnowModel is a numerical model for the spatially-distributed simulation of snow evolution with an explicit consideration of the main physical processes that shape the seasonal snowpack (Liston and Elder, 2006a). The model consists of four modules: a module that interpolates meteorological variables recorded at specific locations to a two-dimensional grid using specially developed algorithms (MicroMet) (Liston and Elder, 2006b); a module that solves the energy balance and yields surface sublimation and snowmelt (EnBal) (Liston, 1995); a module that solves the internal changes of the snowpack, such as refreezing, densification and metamorphism (SnowPack) (Liston and Hall, 1995); and a module that solves the snow transport and blowing snow sublimation due to saltation and suspension of the snow (SnowTran-3D) (Liston et al., 1998). The model does not include a representation of snow gravitational transport. SnowModel has been successfully tested in several snow environments around the world (Liston et al., 2007; Mernild et al., 2016), including the semiarid Andes (Gascoin et al., 2013; Réveillet et al., 2020; Voordendag et al., 2021). Readers are referred to other studies for a full description of the model (Liston and Elder, 2006a) and its updates (Mernild et al., 2018; Merkouriadi et al., 2021).

In SnowModel, snowmelt either refreezes at low layers or drains as runoff when the snowpack has already reached a ripe state. In our study, we analyze results from snowmelt runoff (snowmelt leaving the snowpack) and snow surface sublimation (extracted from the surface turbulent latent heat flux). Rain on snow contributes to a snow density increase, but we do not consider it in the snowmelt runoff variable. We define the sublimation ratio (SublRatio) as shown in Eq. (1):

$$SublRatio = \frac{Snow\ surface\ sublimation}{Snow\ surface\ sublimation + Snowmelt\ runoff} \quad (1)$$

Glaciers can be included in SnowModel as a type of surface and ice is melted once the snow has completely disappeared from the surface. Debris-covered and rock glaciers are not included in the model.

4.2 Setup

We run SnowModel in the Corrales basin using a 3 h timestep in the period April 2019-March 2021. The domain of the model runs is a rectangle that contains the Corrales basin with an additional buffer of 500 m in all four main directions (N-S-E-W).

https://doi.org/10.5194/hess-2023-23
Preprint. Discussion started: 31 January 2023


Hydrology and Earth System Sciences
Discussions

We use a DEM of a spatial resolution of 50 m that is bilinearly resampled from NASADEM (see Section 3.3). The land cover of the model domain consists entirely of bare soil except for the debris-free glaciers shown in Figure 1b.

Table 3: Parameters values used in the SnowModel simulations

Module	Parameter	Value or source	Units
General	Spatial resolution	50	m
	Time step	3	h
	Number of grid cells (East, North)	270, 272	
Meteorological inputs	Precipitation	TAP	mm
	Air temperature	TAP, TGL, PAN	°C
	Relative humidity	TAP, TGL, PAN	%
	Wind speed and direction	TAP, TGL, PAN	m s^{-1} and °
	Solar radiation	TAP	W m^{-2}
	Incoming longwave radiation	TAP	W m^{-2}
	Air pressure	PAN	Pa
MicroMet	Curvature length scale	500	m
	Slope weight for wind distribution	0.58	
	Curvature weight for wind distribution	0.42	
	Monthly mean air temperature lapse rates	From January to December: 8.1,8.1,7.7,6.8,5.5,4.7, 4.4,5.9,7.1,7.8,8.1,8.2	°C km^{-1}
	Precipitation and wind speed lapse rate	0	
Enbal	Albedo decay melt conditions	0.024	s^{-1}
	Albedo decay cold conditions	0.008	s^{-1}
	Glacier albedo	0.3	
	Albedo fresh snow	0.9	
	Soil albedo	0.14	
	Precipitation threshold for albedo reset	0.006	m
	Aerodynamic surface roughness length for snow (z_0)	0.001	m
SnowPack	Number of layers	6	
SnowTran-3D	Threshold surface shear velocity	0.25	ms^{-1}

235

https://doi.org/10.5194/hess-2023-23
Preprint. Discussion started: 31 January 2023


Hydrology and Earth System Sciences
Discussions

We run the model using mostly default model parameters (Table 3) and without performing any calibration except for the albedo decay rates, which were manually set to fit the albedo changes observed at TAP (Figure S4). The model is forced using the meteorological data described in Section 3.1. The wind speed records were adjusted from the corresponding sensor height to a height of 2 m using a logarithmic wind profile and an aerodynamic surface roughness length for snow of 5 mm.

4.3 Ensemble runs

We produce ensemble runs with the characteristics described in Table 3 and considering three different values for three selected variables: a precipitation factor, the aerodynamic surface roughness length for snow and two wind distribution weights based on the slope and curvature of the terrain in the MicroMet module. The aerodynamic surface roughness length (hereafter z_0) is a key parameter controlling the mass and energy exchanges between the surface and the atmosphere and has been defined as the height above a surface at which the extrapolated horizontal wind-speed profile reaches zero (Brock et al., 2006). According to the MicroMet module, the slope and curvature wind distribution weights should sum to one. Previous snow simulations in this area have resulted to be most sensitive to these variables (Réveillet et al., 2020; Voordendag et al., 2021). We test all the different combinations of these values, obtaining a total of 27 simulations that are used to assess model sensitivity and uncertainty. Table 4 provides a summary of the values and variables in the ensemble runs.

Table 4: Summary of SnowModel ensemble runs

Parameters and configuration	Values
Precipitation factor	0.7
	1.0
	1.3
Aerodynamic surface roughness length for snow (z_0) (m)	0.001
	0.005
	0.010
Slope (curvature) weight	0.25 (0.75)
	0.58 (0.42)
	0.75 (0.25)
Other parameters	As in Table 3

5 Results

5.1 Analysis of snow products

The maps of the SA and SP indices show the areas that are prone to remaining snow-free during the accumulation period and the areas where snow persists during the melt period, respectively (Figure 3). While high SA values are found at ridges and

https://doi.org/10.5194/hess-2023-23
Preprint. Discussion started: 31 January 2023

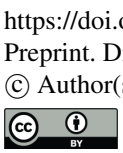

Hydrology and Earth System Sciences
Discussions

sites located at the east of the catchment, low values are found at valley bottoms that are mostly located at the west of the catchment (Figure 3a). Polar plots in Figure 3b show the relationship between elevation, aspect and the SA index. In general, sites higher than 4000 m a.s.l. with a SW-S-SE orientation are snow-covered during the accumulation period (SA<0.5). On the contrary, sites located with a N, NW and NE aspects have the highest values of SA, which suggests a strong role of solar radiation even in the period of the year with the lowest radiation values. Approximately 15% of the catchment is snow-free during the accumulation period (SA close to one, Figure 3c). The map of SP shows that the Corrales catchment is mostly snow-free during summer (Figure 3d), except for sites above 4500 m a.s.l. with S and SW aspects (SP>0.2, Figure 3e). Approximately 45% of the catchment is almost always snow-free during the melt period (SP close to zero, Figure 3f). Glaciers appear as areas of minimum SA (Figure 3a) and maximum SP (Figure 3d).

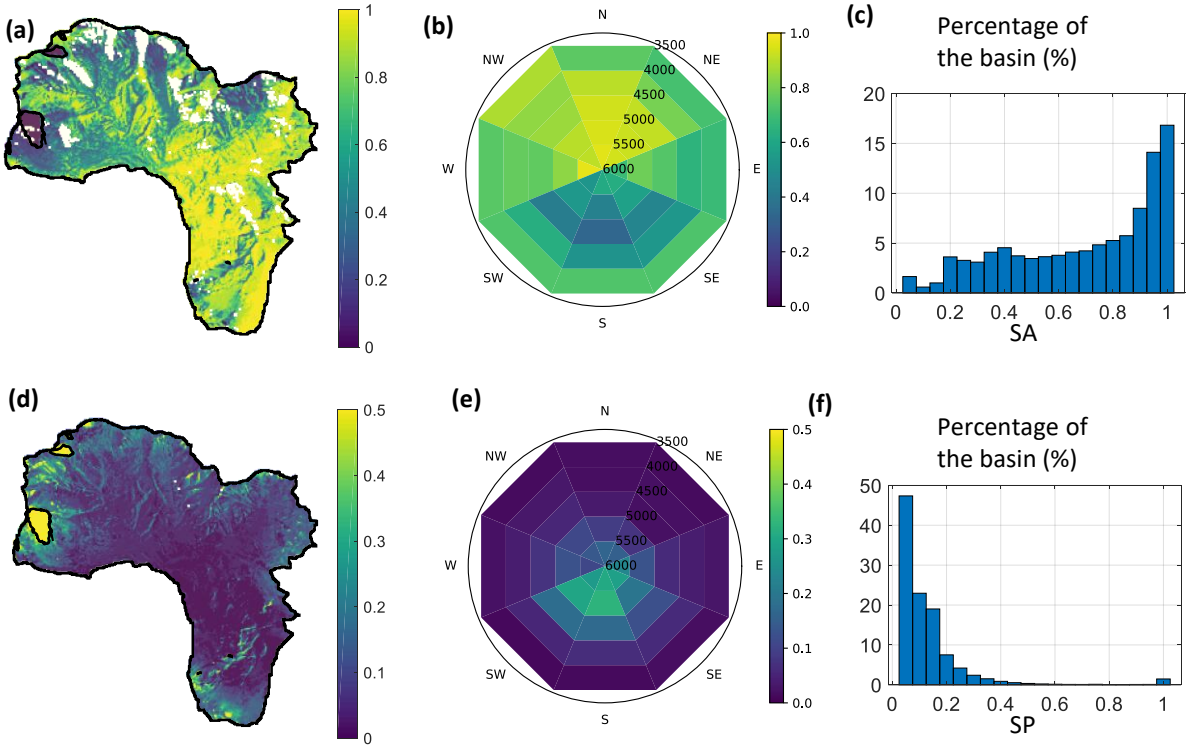

Figure 3: SA and SP indices in the Corrales basin calculated over the study period using the methodology developed by Wayand et al. (2018)**. (a) Map of SA, (b) Polar plot of SA, (c) Histogram of SA values, (d) Map of SP, (e) Polar plot of SP, (f) Histogram of SP values. Glaciers outlines are shown in (a) and (d).**

In Figure 4 we analyze the SWE reconstruction of Cortés and Margulis (2017) for our study catchment in the period 1985-2015. While Figures 4a-c present the interannual median of the annual maximum SWE, Figures 4d-f show the coefficient of variation of the same variable. The highest values of maximum SWE are found over westerly areas, close to Tapado Glacier, whereas maximum SWE values are very low in eastern sections (Figure 4a). Figure 4b shows that maximum SWE values are highest at sites between 4500 and 5000 m a.s.l. with SW-S-SE aspects and between 5000 and 5500 m a.s.l. with a S aspect. This is an indication of sites with preferential snow deposition. The snowpack of the catchment is relatively shallow with only

https://doi.org/10.5194/hess-2023-23
Preprint. Discussion started: 31 January 2023

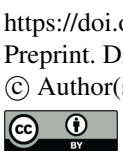

Hydrology and Earth System Sciences
Discussions

ca. 5% of the area having maximum SWE > 200 mm w.e. (Figure 4c). The coefficient of variation of maximum SWE reaches values up to 4.5, particularly at the east of the catchment, at sites > 4500 m a.s.l. with N aspects (Figures 4d-e). Almost 75% of the catchment area has a coefficient of variation >1, which is in line with the high interannual variability of precipitation in this region. Glaciers are located in areas of high snow accumulation (Figure 4a) and low coefficients of variation (Figure 4d).

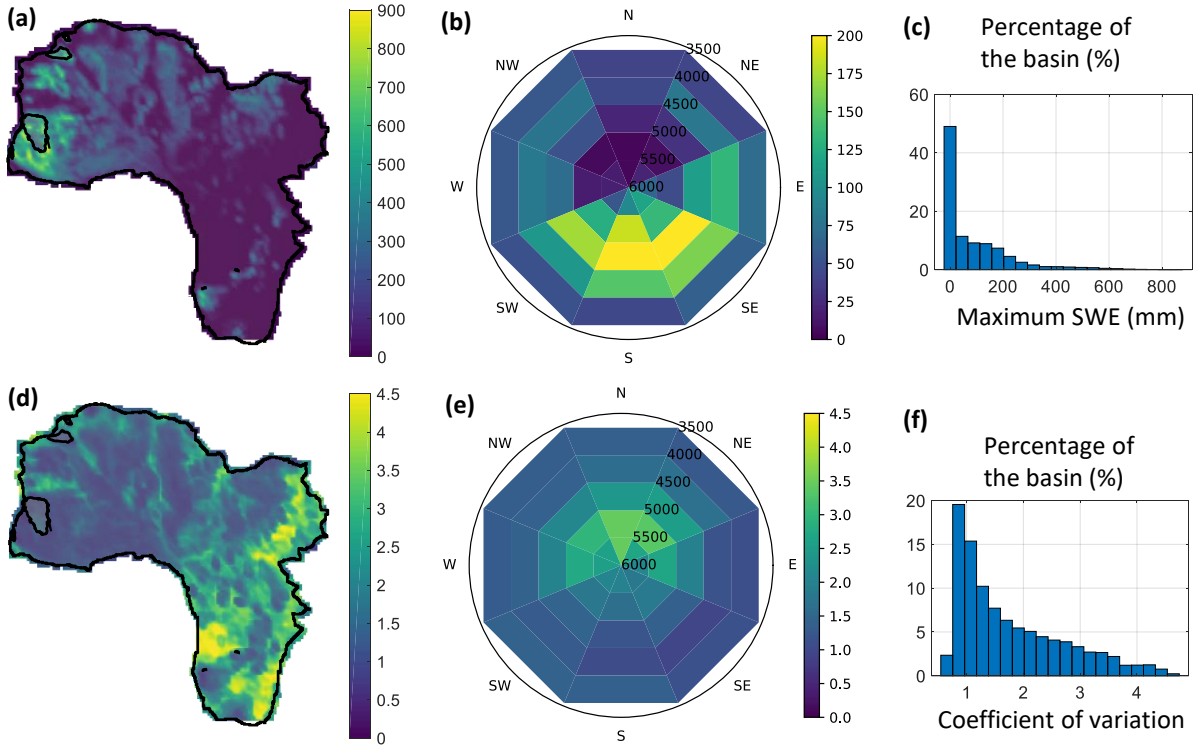

Figure 4: Annual maximum snow accumulation in the Corrales basin during 1985-2015 according to the daily SWE reconstruction by Cortés and Margulis (2017)**. (a) Map of the interannual median, (b) Polar plot of the interannual median, (c) Histogram of the interannual median, (d) Map of the coefficient of variation, (e) Polar plot of the coefficient of variation, (f) Histogram of the coefficient of variation. Glaciers outlines are shown in (a) and (d).**

5.2 Verification of SnowModel results

In Figure 5, we compare results of SnowModel ensemble runs against measurements of snow depth and SWE at TAP. Model results are in good agreement with both independent records. The simulated changes of snow depth following precipitation events are similar to observations, particularly during periods of rapid depletion following each precipitation event. Rapid depletion periods are likely due to compaction, as well as mechanical removal and sublimation caused by frequent strong wind gusts and rapid drops in humidity occurring post precipitation. We discarded that these drops are caused by melt because air temperature was very low following events. We also observe differences in the modeled and observed peak snow depth and SWE that are likely caused by discrepancies between the precipitation amounts registered by the Geonor sensor and the snow

https://doi.org/10.5194/hess-2023-23
Preprint. Discussion started: 31 January 2023

Hydrology and Earth System Sciences
Discussions

records. The snow disappearance date is well approximated in October 2019, September 2020 and October 2020 in the snow depth record (Figure 5a), but the SWE observations show a slower disappearance rate.

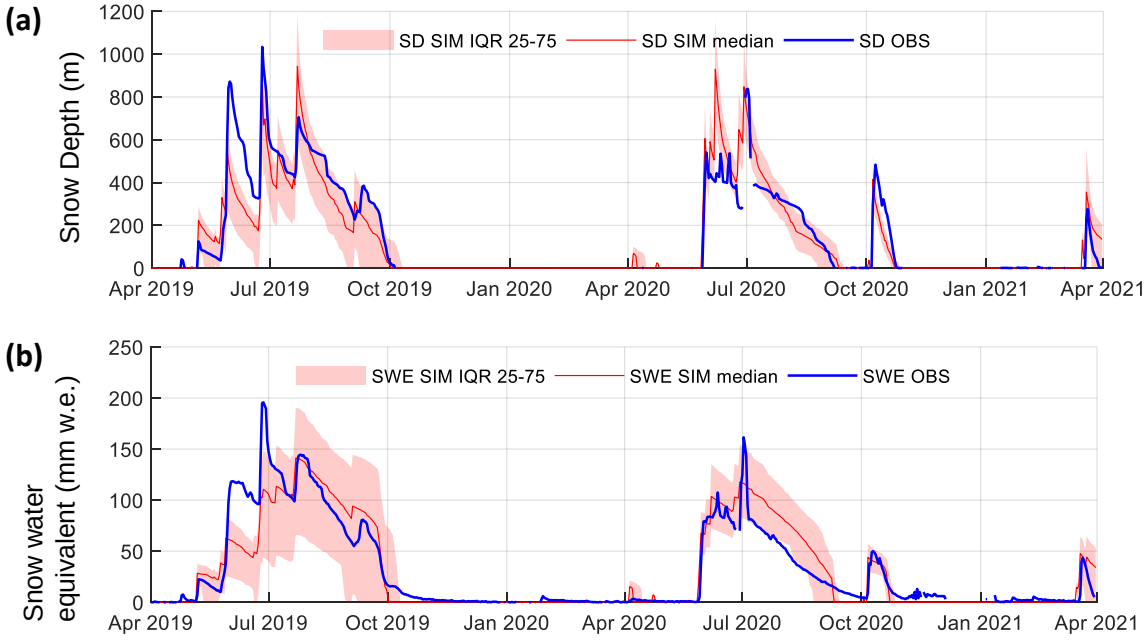

Figure 5: Time series of the observed and simulated snow variables at TAP. (a) Snow depth, (b) SWE. The red lines and areas represent the median values and interquartile ranges 25 and 75 of the SnowModel ensemble runs, respectively. The blue lines correspond to the observations.

A comparison of observed and simulated snow variables at the distributed scale is presented in Figure 6. Figure 6a shows SCA from the ensemble runs (red area and line) against SCA derived from Sentinel-2A (blue points). The SCA from the ensemble runs coincides well with the Sentinel-2A values at several times throughout the study period, but the snow disappears too early in the simulations. Figures 6b-c show the comparison between SA and SP derived from satellite images and from SnowModel. The SnowModel values of SA and SP follow the same definitions of the satellite-derived indices but using the results of the simulations. In correspondence to the polar plots presented in Figures 3 and 4, each point in Figures 6b-c represents the SA and SP average value of all the grid cells contained in a 500-m elevation band (from 3500 to 6000 m, 5 values in total) and 45° aspect (from N to NW, 8 values in total), whereas the error bars represent SA and SP standard deviation over the same grid cells. There is a good correlation between observed and simulated values (R^2=0.47 for SA and R^2=0.64 for SP), although the absolute numbers do not coincide. This is a consequence of comparing satellite-derived indices from images that are available only every 2 to 3 weeks, and model-derived indices that are calculated using every 3h time step. In Figure 6b, the two data points that do not align in the general linear relationship (lower right corner) correspond to sites located to above 5500 m a.s.l. with an E and SE aspect. Figure 6d shows the same plots but comparing the interannual medians of simulated and reference (Cortés and Margulis, 2017) SWE at the time of annual maximum accumulation. While the interannual median

https://doi.org/10.5194/hess-2023-23
Preprint. Discussion started: 31 January 2023

Hydrology and Earth System Sciences
Discussions

of the reference values are calculated from the 1985-2015 period, the interannual median of simulated values is calculated using the two hydrological years of the modelling period (2019-2020 and 2020-2021). The correlation between both records is lower than that of the snow indices (R^2=0.25), likely due to difficulties of SnowModel to reproduce the shallow and deep snowpacks produced by the reference dataset.

In Figure 7 we compare simulated values of surface mass balance on the lowest section of the debris-free Tapado Glacier (below 4800 m a.s.l.) against the set of ablation stakes readings (Section 3.1). The surface glacier mass balance of this area is calculated using snow accumulation and erosion (snowfall and wind transport), snow ablation (surface sublimation, blowing snow sublimation and snowmelt runoff) and ice melt and sublimation. As the ablation measured at the stakes and that of their corresponding model grid cells might differ due to topographic differences between the sites and that of the 50-m resolution DEM, we prefer to compare all the stakes readings against spatially averaged values over the glacier tongue. Although there are some differences between observed and simulated values, the main trends throughout the season are similar, with a higher ablation rate between November and February and a reduced rate after March.

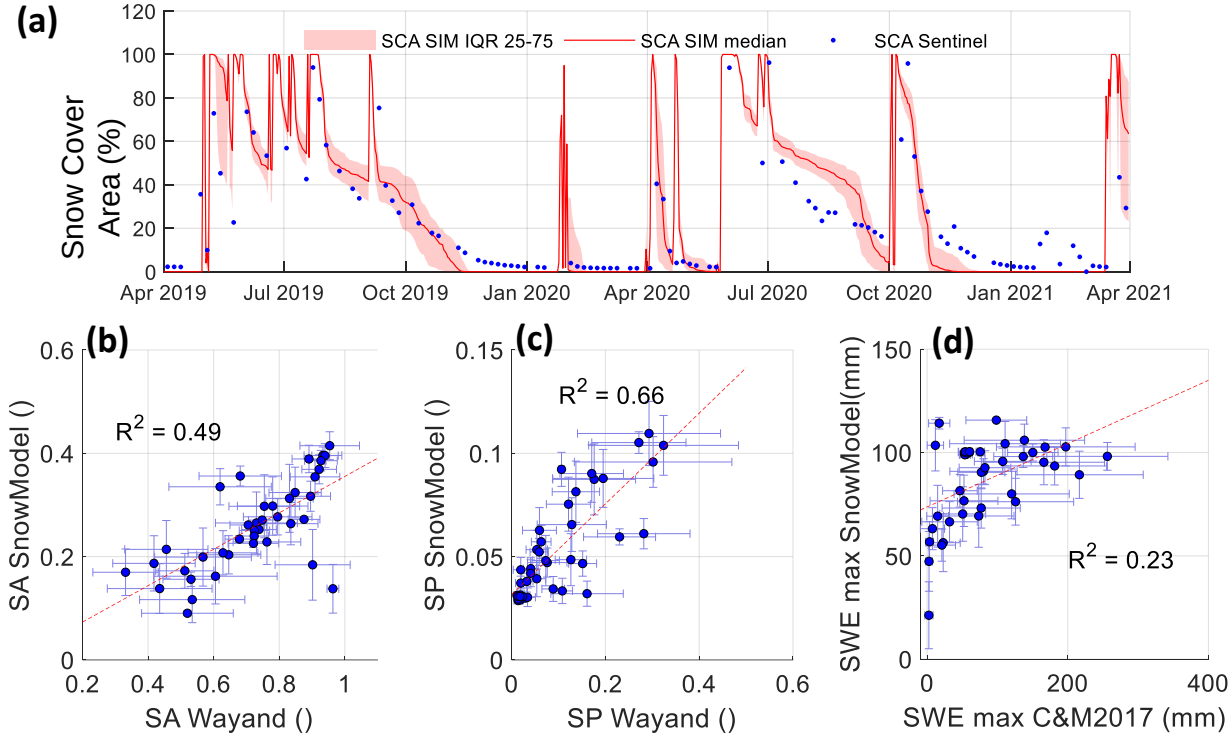

Figure 6: Comparison of the observed and simulated snow variables at the scale of the Corrales catchment. (a) Snow cover area, (b) SA, (c) SP, and (d) annual maximum snow accumulation. In (a) the red lines and areas represent the median values and interquartile ranges 25 and 75 of the SnowModel ensemble runs, respectively. The blue lines correspond to the observations. In b-d the blue points and error bars represent the mean and standard deviations values, respectively, within a 500-m elevation band (from 3500 to 6000 m a.s.l.) and a 45° aspect range (from 22.5° to 337.5°) as the polar plots in Figures 3 and 4.

https://doi.org/10.5194/hess-2023-23
Preprint. Discussion started: 31 January 2023

Hydrology and Earth System Sciences
Discussions

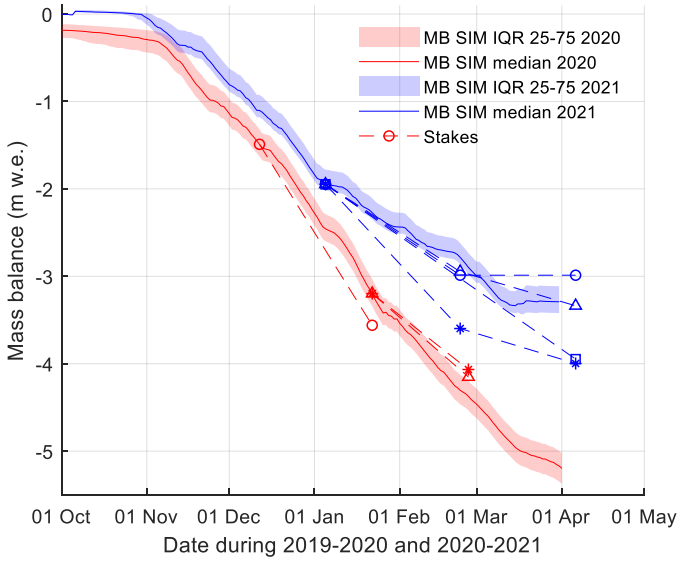

Figure 7: Comparison of the simulated cumulative mass balance of the ablation area of Tapado Glacier against ablation stakes readings in the period October-April of years 2019-2020 and 2020-2021. The red and blue lines and areas represent the median values and interquartile ranges 25 and 75 of the SnowModel ensemble runs, respectively. The markers correspond to the ablation stakes readings and the dashed lines are connecting lines that help visualization. To help comparison, we set the first marker of each line at the simulated mass balance value in that date. The cumulative mass balance is set at zero on April 1 of each year.

5.3 Snow mass balance and runoff generation

Figure 8 shows the catchment-average snow mass fluxes in the study period calculated as the median of the SnowModel ensemble runs. Precipitation occurred mostly in autumn and winter (April to June) with some extraneous events in September 2019, January 2020, October 2020 and March 2021. Rainfall was much lower than snowfall and was mostly restricted to summer and autumn. Snow surface sublimation was the process that removed most of the snow mass and dominated ablation during winter and spring. Snowmelt runoff and ice melt played a secondary role at the annual level, but their relative importance increased in spring and summer, respectively. From November to March, ice melt was almost the only runoff contributor. Fluxes derived from the transport of snow (wind-transported snow and blowing snow sublimation) were small and took place only during winter or other periods with fresh snow on the surface. While blowing snow sublimation is always a mass loss (negative values), wind-transported snow can add or remove mass to the catchment (positive or negative values), but in the study period it was mostly a mass loss.

https://doi.org/10.5194/hess-2023-23
Preprint. Discussion started: 31 January 2023

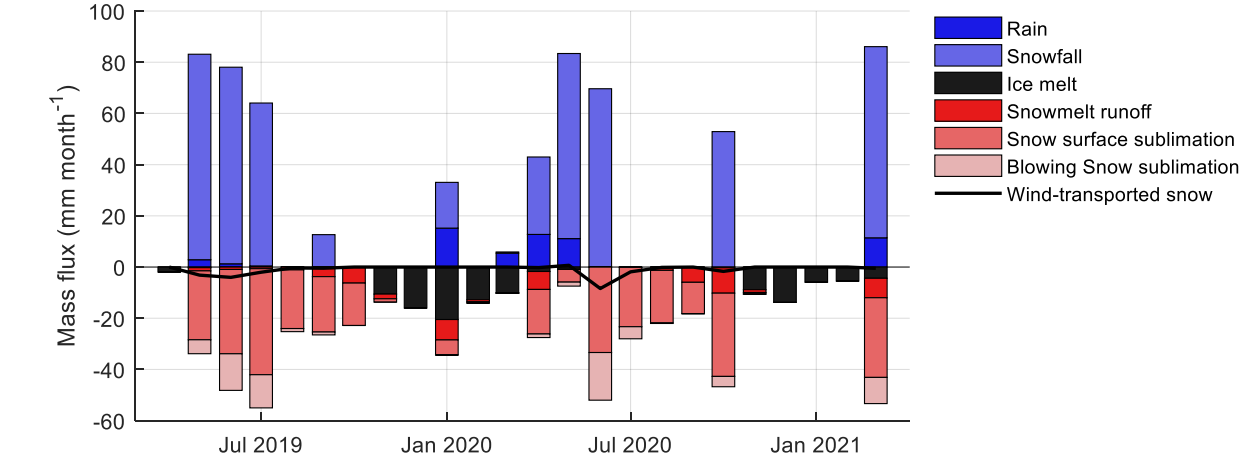

Figure 8: Monthly mass fluxes in the Corrales catchment. Liquid and solid precipitation are considered as inputs to the catchment (plotted as positive bars), whereas ice melt, snowmelt runoff, surface sublimation and blowing snow sublimation are considered as losses from the catchment (plotted as negative bars). Wind-transported snow is the sum of suspension and saltation and can be both an input and an output (plotted as a black line).

Figure 9 presents maps and polar plots of the ensemble runs medians of snowmelt runoff, snow surface sublimation and sublimation ratio. Snowmelt runoff is concentrated at wind-sheltered sites located on the west side of the catchment (Figure 9a), particularly at sites located between 4000 and 4500 m a.s.l. with E and SE aspects (Figure 9d). Snow surface sublimation occurs mostly at wind-exposed locations (Figure 9b), largely dominating total ablation on the east side of the catchment (large values of sublimation ratio in Figure 9c). Figure 9e shows that snow surface sublimation increases with elevation reaching its maximum values at sites located above 5500 m a.s.l. with a W, NW and SW aspect. The lowest values of sublimation ratio, i.e. where snowmelt runoff is more important than sublimation, are slightly above 50% and are located in the valleys on the west side of the catchment (Figure 9c), mostly at sites between 4000 and 4500 m a.s.l. with E and SW aspects (Figure 9f). Glaciers appear as sites dominated by snow surface sublimation with a large sublimation ratio (Figure 9c). However, in terms of runoff volume, ice melt corresponds to 61% of total ablation (snowmelt and ice melt), which is equivalent to 4.3 $Mm^3\ a^{-1}$. In Figure 10 we compare snowmelt runoff and snow surface sublimation over the catchment and its glaciers using boxplots calculated with the SnowModel ensemble runs. Snow surface sublimation is the largest mass loss from the catchment reaching values between 100 and 250 mm a^{-1} (Figure 10a) and represents between 71 to 94% of total ablation (Figure 10b). We find that snowmelt runoff at the catchment level and ice melt have similar mean values (between 34 and 55 mm a^{-1}), but the uncertainties derived from our ensemble runs are much larger for snowmelt runoff than for ice melt (Figure 10a). In Figure 10a, the boxplots for debris-free glaciers are made using values averaged over glacier grid cells. These results show that snow surface sublimation over glaciers is larger than the catchment average, but the sublimation ratio is similar (Figure 10a-b). We find that 50% of the snowmelt runoff is generated from 18-28% of the catchment area (Figure 10c), which we identify as snowmelt hotspots. Another interesting result is that 50% of the catchment produces ca. 80% of the total snowmelt runoff

https://doi.org/10.5194/hess-2023-23
Preprint. Discussion started: 31 January 2023

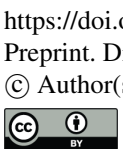

Hydrology and Earth System Sciences
Discussions

(Figure 10c). In Figure 10d, we show a map of the snowmelt hotpots calculated as the minimum area that produces 50% of the snowmelt runoff in the catchment (calculated from the median of the SnowModel ensemble runs). Using this definition, none of the debris-free glaciers correspond to snowmelt hotspots.

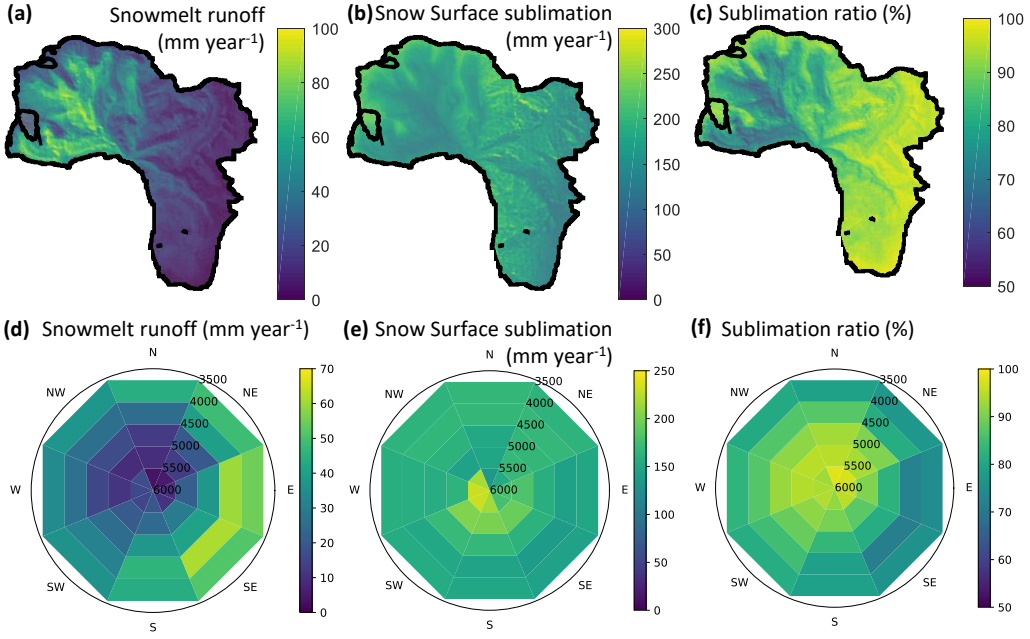

Figure 9: Maps and polar plots of snow mass fluxes calculated as the medians of the SnowModel ensemble runs for 2019-2021. (a) Snowmelt runoff, (b) Snow surface sublimation, (c) Sublimation ratio.

Figure 11 shows the importance of different factors that control the location of snowmelt hotspots by comparing the cumulative distribution functions of different descriptive variables of snowmelt hotspots and the rest of the catchment. Snowmelt hotspots are located below 5250 m a.s.l., (mostly between 4200 and 4800 m a.s.l., Figure 11a), have a E, NE and SE aspect (ca. 80% of the snowmelt hotspots have an aspect lower than 180°, Figure 11b) and low slope angles (Figure 11c). In terms of snow variables, snowmelt hotspots show snow depth values at the time of maximum accumulation of at least 0.7 m (Figure 11d), with SA values lower than 0.3 (Figure 11e) and SP values of at least 0.03 (Figure 11f).

The relationship between snowmelt runoff and snow surface sublimation to the selected inputs in Table 3 is assessed using an R-squared analysis of the ensemble runs (Table 5). Ensemble variability in snowmelt runoff is mostly explained by z_0 (R^2=0.72) and less so by precipitation (R^2=0.11). Snow surface sublimation ensemble variability presents an almost opposite behavior being mostly explained by precipitation (R^2=0.65) and less so by z_0 (R^2=0.29). Interestingly, we find that snowmelt runoff is better explained by z_0 than snow surface sublimation is. In fact, as snow surface sublimation is the largest flux in the snow mass balance of the catchment, this variable is mostly explained by total precipitation. Consequently, sublimation ratio is not related to total precipitation, and it is almost completely dependent on z_0 (R^2=0.85).

https://doi.org/10.5194/hess-2023-23
Preprint. Discussion started: 31 January 2023

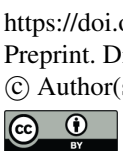

Hydrology and Earth System Sciences
Discussions

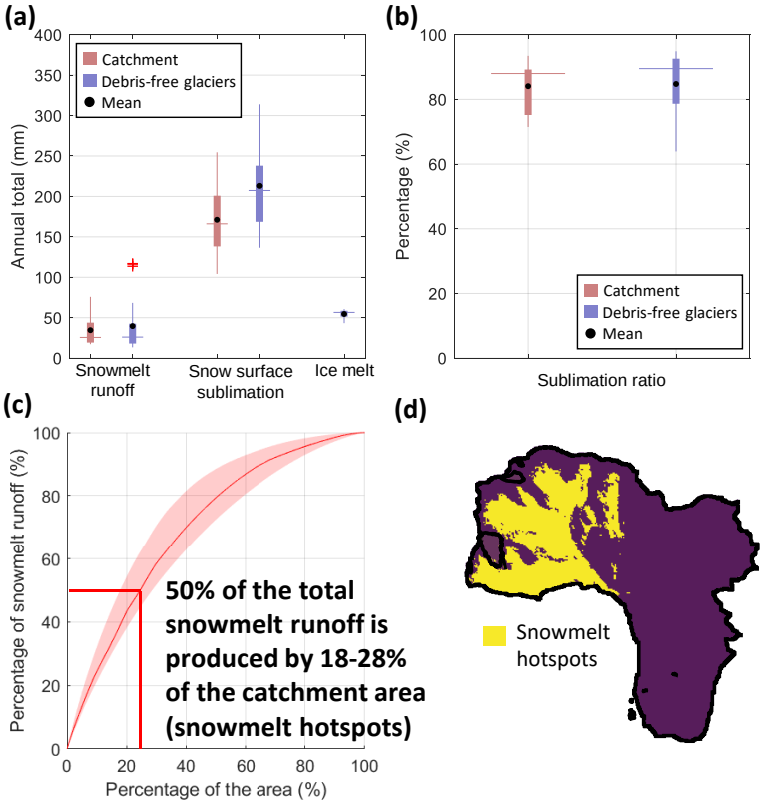

Figure 10: (a-b) Boxplots of snowmelt runoff, snow surface sublimation, ice melt and sublimation ratio in the Corrales catchment (red boxplots) and debris-free glaciers (blue boxplots), (c) Cumulative snowmelt and area, (d) Map of snowmelt hotpots. Boxplots are built using the SnowModel ensemble runs. In (a) ice melt values are normalized by the catchment area. The edges of the boxes represent the 25th and 75th percentiles, the horizontal lines represent the median and the black dots corresponds to the mean. Outliers are shown with a red cross. In (c) the red lines and areas represent the median values and interquartile ranges 25 and 75 of the SnowModel ensemble runs, respectively.

https://doi.org/10.5194/hess-2023-23
Preprint. Discussion started: 31 January 2023

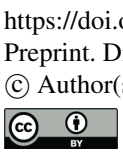

Hydrology and Earth System Sciences
Discussions
Open Access
EGU

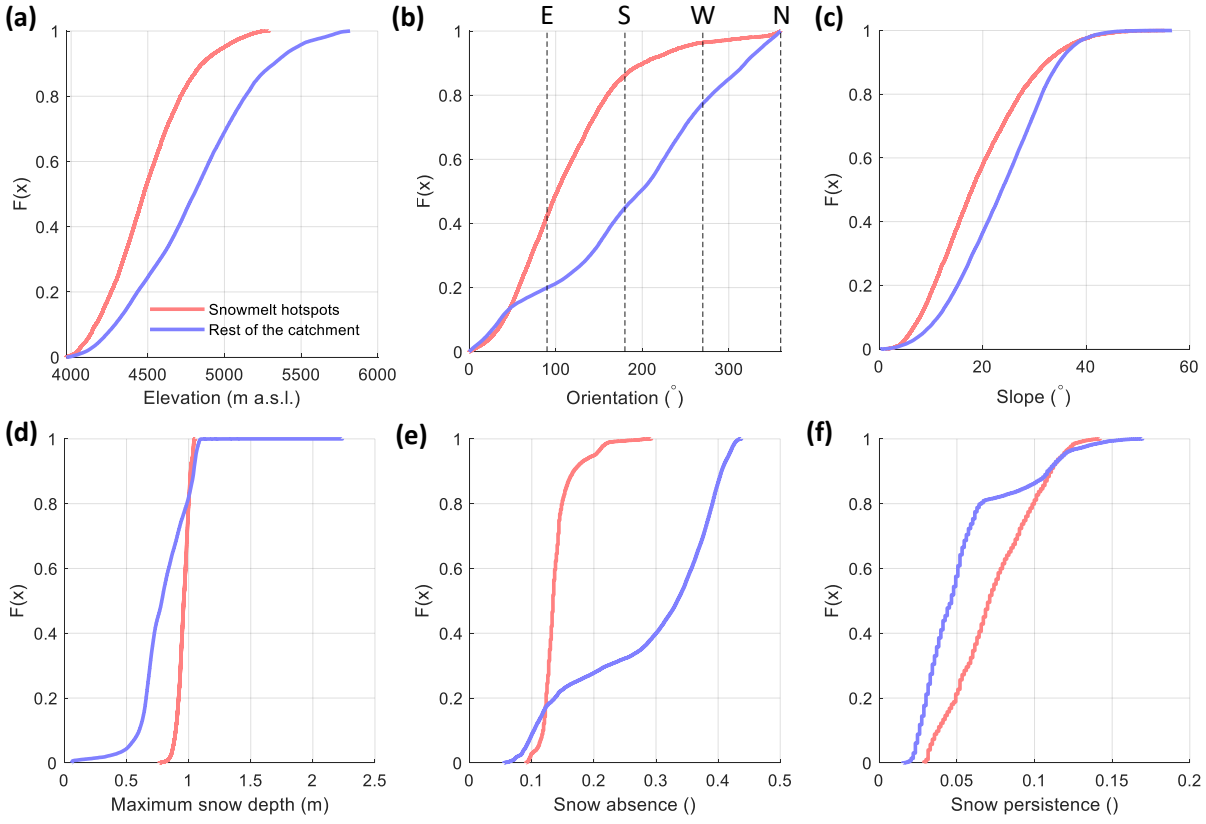

405 **Figure 11: Cumulative distribution functions (CDFs) of selected topographic and snow variables for snowmelt hotspots and the rest of the catchment (except hotspots). In upper part of (b) we add cardinal directions in letters for reference.**

410 **Table 5: R-squared values of linear regressions between SnowModel parameters and outputs**

		Model inputs		
		Precipitation factor	Aerodynamic surface roughness length for snow (z_0)	Wind factor
Model outputs	Snowmelt runoff	0.11	0.72	0.00069
	Snow surface sublimation	0.65	0.29	0.00019
	Sublimation ratio	0.03	0.85	0.00039

In Figure 12 we assess the snow fluxes derived from the snow transport by wind. Wind-transported snow is close to zero on the west side of Corrales catchment and varies between positive (snow deposition) and negative (snow erosion) values to the east (Figure 12a). Snow erosion (negative values) dominates over deposition at sites located between 4500 and 5500 m a.s.l.

https://doi.org/10.5194/hess-2023-23
Preprint. Discussion started: 31 January 2023

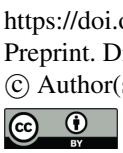

Hydrology and Earth System Sciences
Discussions

415 with W, NW and N aspects (Figure 12c). Blowing snow sublimation is also close to zero on the west side of the catchment and reaches values of up to −100 mm a^{-1} to the east (Figure 12b), particularly at sites above 4500 m a.s.l. with W, NW, N and NE aspects (Figure 12d).

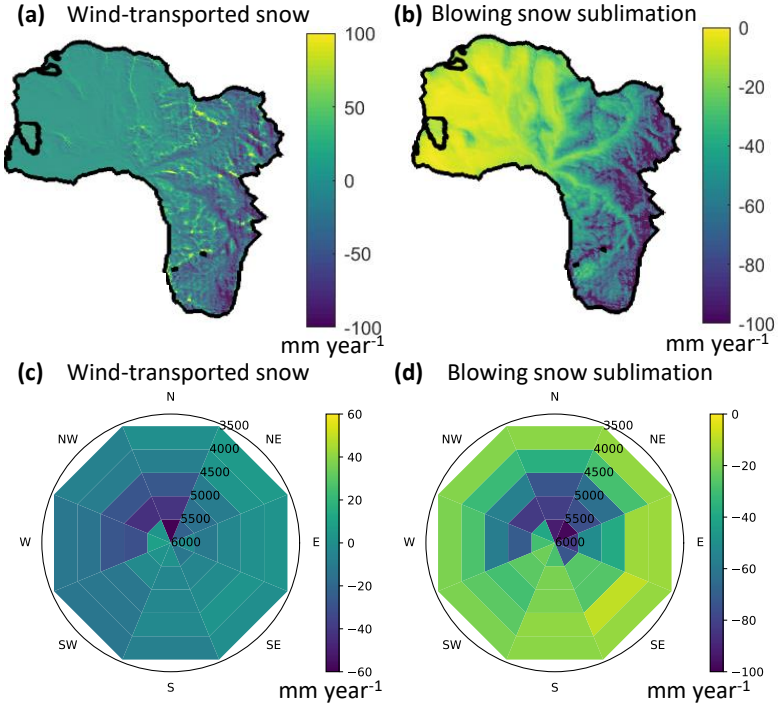

420 **Figure 12: Annual maps and polar plots of snow mass fluxes calculated as the medians of the SnowModel ensemble runs. (a) Snowmelt runoff, (b) Snow surface sublimation, (c) Sublimation ratio.**

6 Discussion

6.1 Verification of model results

The seasonal amounts of snow observed at TAP are well reproduced by SnowModel, but the simulations fail to match the 425 magnitude of some of the accumulation peaks, particularly in terms of snow depth during the winter 2019 (Figure 5a). Most of the depletion curves are well captured by the model simulations, except for the depletion curve in the spring 2020, which does not follow the same rates shown by the snow depth and SWE (Figure 5a-b). As suggested by Voordendag et al. (2021) when analyzing the TAP station site in winter 2017, these differences are likely given by the uncertainty in the precipitation forcing and the parametrization of fresh snow density and albedo. Additionally, model results reproduce the main patterns of 430 glacier ablation on the tongue of Tapado Glacier, although more detailed parameterizations are certainly needed to simulate the energy and mass balance on penitentes fields in their full complexity (Lhermitte et al., 2014; Sinclair and MacDonell, 2015; Nicholson et al., 2016).

https://doi.org/10.5194/hess-2023-23
Preprint. Discussion started: 31 January 2023


Hydrology and Earth System Sciences
Discussions

Model results are also in good agreement with distributed datasets. We find that the snow indices proposed by Wayand et al. (2018) are particularly useful to evaluate our results as they provide additional information on the spatial distribution and duration of the snow, in contrast to analyses based solely on the percentage of SCA in the study basin. The correlation between observed and simulated SA is lower than that of SP (R^2=0.49 versus R^2=0.66, Figure 6b-c). This result is expected because SA is controlled by accumulation processes that are difficult to reproduce in snow models, such as wind fields over complex terrain and preferential deposition (Mott et al., 2010; Freudiger et al., 2017; Hock et al., 2017). The poorer performance of the model in the accumulation season can also be observed in the low correlation (R^2=0.23) between the annual maximum accumulation from the model and the SWE reconstruction dataset that we use as reference (Cortés and Margulis, 2017). This low correlation is in part explained by the large spread of simulated maximum SWE values when compared against low values of the reference dataset (Figure 6d). This is likely caused by the simulation of low wind speeds and large snow accumulation at sites dominated, in reality, by snow erosion and high wind speeds. On the other hand, a correct representation of SP is more easily achieved because this index is more related to ablation processes that depend on variables that are easier to reproduce, such as solar radiation and air temperature gradients (Wayand et al., 2018). However, despite the good correlation between the observed and simulated SP, the snow cover disappears earlier in the simulations than in the satellite images (Figure 6a). This is likely caused by insufficient snow accumulation simulated by the model at high-elevation sites, whereas in reality snow can remain on the surface until the start of the summer (December).

A key advantage of our study is the use of well-distributed AWS data to force the snow simulations, particularly the contrasting wind records of PAN and the rest of the AWSs, which are located at wind-exposed and wind-sheltered locations, respectively. In fact, some differences between our simulations and those of Réveillet et al. (2020) might be caused by the unavailability of those records during long time periods of their study. For example, we obtain much larger sublimation ratios compared with their simulations resulting from a similar AWS forcing (~85% versus ~35%). Similarly, Gascoin et al. (2013) obtained a sublimation ratio of ca. 70% applying SnowModel to an instrumented site in Pascua-Lama (2600–5630 m a.s.l., 29°S) over the 2008 winter. Another good indication for our simulations are the results of point-scale studies on glaciers of the semiarid Andes, such as those from Ginot et al. (2006) and MacDonell et al. (2013), which obtained year-round sublimation ratios around 80% on the upper areas of Tapado and Guanaco (5324 m a.s.l., 29.34°S, 70.01°W) glaciers, respectively. On the other hand, Ayala et al. (2017b) obtained a sublimation ratio of 12% on the tongue of Tapado Glacier, but those results were obtained from a two-month summer period.

6.2 Snowmelt hotspots and hydrological significance

In relation to the main hypothesis of this study, i.e. the existence of snowmelt hotspots in the semiarid Andes, we have identified the areas that produce half of the snowmelt runoff in the Corrales catchment, and described their main topographic and meteorological characteristics. We estimate that these areas correspond to 18-28% of the catchment area. Although we use a threshold of 50% to define the snowmelt hotspots, alternative definitions might be applied in the future depending on the objectives of each study. These results are in line with other studies showing how the heterogeneity of snow processes affect

https://doi.org/10.5194/hess-2023-23
Preprint. Discussion started: 31 January 2023


Hydrology and Earth System Sciences
Discussions

runoff generation (DeBeer and Pomeroy, 2017). The hydrological relevance of snowmelt hotspots can also be connected with the results from Badger et al. (2021), that used idealized simulations to show that the heterogeneity of the snow cover delays snowmelt runoff and creates areas of snow persistence. We suggest that in other arid or semiarid catchments, snowmelt hotspots could be expected for leeward slopes with relatively low slope angles and moderate elevations. Snow persistence might be an indicator for such hydrologically relevant sites. However, to precisely identify snowmelt hotspots and quantify their contribution in other regions, a modeling approach combined with satellite information should be applied such as the one presented in this work.

Snowmelt hotspots in the semiarid Andes are a clear illustration of the large spatial variability of physical processes (from accumulation to heat exchange) that ultimately control snowmelt runoff (Mott et al., 2018). First, the sheltering and exposure to strong winds during and after snowfall events determine large differences in snow accumulation, from areas of preferential deposition, such as glacier accumulation zones, to large areas of strong snow erosion by the wind and shallow snowpacks (Figures 3 and 4). In this direction, other phenomena, such as mesoscale lowering of the 0°C isotherm have also been suggested as important for snow accumulation in this type of environment (Schauwecker et al., 2022). Second, the high sublimation rates (of up to 300 mm a^{-1}, Figure 9) use large amounts of energy from the snowpack that would be otherwise available for melt. The combination of these two factors define an heterogeneous snow cover in which snow-free areas appear very early in the melting season (ca. 50% of the catchment area in August, Figure 6a), likely contributing to snowmelt through the advection of sensible and latent heat (Liston, 1995; Mott et al., 2020; van der Valk et al., 2022). A logical step towards improving our estimates of snowmelt runoff in this type of environment would be the calculation of the contribution of local heat advection from snow-free areas to snowmelt rates. Other studies have estimated a contribution of up to 40% in alpine, prairie and arctic environments (Mott et al., 2018).

In regions where snow sublimation is less important in the water balance or restricted to specific locations (e.g. Strasser et al., 2008), snowmelt runoff is expected to originate in areas with large snow accumulation. We here show that this is not necessarily the case in environments with high sublimation rates. This is an important finding for hydrological modelling and water management, since not all sub catchments with snow cover during winter contribute the same way to available water downstream during e.g. the irrigation season. Future snow monitoring in the semiarid Andes should thus focus especially on sites where large part of snowmelt is generated and their connection with other hydrological components. In fact, snowmelt hotspots might play a key hydrological role in connection with other components of this landscape, such as peatlands, groundwater recharge and rock glaciers. Valois et al. (2020) investigated the hydrological dynamics of a mountain peatland in a catchment close to Corrales and found that these features connect snowmelt at high-elevation areas with downstream agriculture and human needs, but there are no estimates of the runoff recharge from the melting of the cryosphere. In this direction, we recommend the assessment of the spatial connectivity between snowmelt hotspots and peatlands. The infiltration of meltwater into rock glaciers is another possible link between snowmelt hotspots and the hydrology of the catchments (Schaffer et al., 2019; Pourrier et al., 2014). Interestingly, Álvarez-Garretón et al. (2021) showed that the hydrological memory of snow-dominated catchments between 30 and 35 °S are strongly influenced by the infiltration of snowmelt at high-elevation.

https://doi.org/10.5194/hess-2023-23
Preprint. Discussion started: 31 January 2023


Hydrology and Earth System Sciences
Discussions

Although glacier runoff is an important component in the water balance of the semiarid Andes (Gascoin et al., 2011; Rodriguez et al., 2016), we found that the main glacier in our study catchment, Tapado Glacier, is not located in an area defined as snowmelt hotspot in this study. However, in line with the results of Gascoin et al. (2013), the snow products analyzed in this study and the results of the SnowModel simulations show that Tapado Glacier is located in an area of preferential deposition and low erosion rates (Figures 3, 4 and 12). Furthermore, our results show that snow sublimation in glacierized areas is very high (Figure 10b), suggesting that sublimation and its associated turbulent latent heat fluxes significantly reduce summer ablation by reducing the energy available for melt. On the other hand, once the snow disappears, the ice surface is quickly melted, creating large amounts of runoff that reach up to 61% of the runoff contributions in the catchment. As the ice melt volume estimate of 4.3 $Mm^3\ a^{-1}$ is relatively high in comparison with other studies (Robson et al. (2022) estimated that the average annual volume change of Tapado Glacier in the period 2012-2015 was of 0.6 Mm^3), we recommend the application of more detailed schemes to solve the energy and mass balance of glaciers in the Corrales catchment.

Although the advantageous location of the AWSs allowed us to capture the main patterns of the spatial variability of the meteorological forcing variables, the total number of stations is still insufficient to capture the full complexity of snow processes in this dry environment. Additionally, future modelling studies will benefit from the inclusion of heat advection from snow-free areas (van der Valk et al., 2022) and time-dependent parameterizations of z_0 (Réveillet et al., 2020; Voordendag et al., 2021). As the period analyzed in this study was very dry, the presence and role of snowmelt hotspots should be analyzed during wet years, where a more uniform distribution of snow accumulation could be expected. However, the hydrological processes that we analyzed in this study might become more frequent in the future, in line with the projections for this region in the context of climate change.

7 Conclusions

In this study we hypothesize and test the existence of areas providing most of the snowmelt runoff in a sublimation-dominated environment in the semiarid Andes. For this we used a process-based snow model (SnowModel) to simulate the evolution of the seasonal snow cover over a two-year period in a 79 km^2 catchment (Corrales catchment) located in the upper areas of the semiarid Andes of Chile. Our main conclusions are as follows:

1. Snow surface sublimation is the dominant ablation component, representing between 71 and 94 % of total ablation.
2. We estimate that 50% of the snowmelt runoff is produced by 18-28% of the catchment area, which we define as "snowmelt hotspots".
3. Snowmelt hotspots are mostly located at elevations between 4200 and 4800 m, have easterly aspects, low slope angles, and high snow accumulation and persistence.

Snowmelt hotspots can be a useful concept to understand runoff generation in this type of environment as it might help to identify the areas of hydrological connections between the components of the catchment, such as the snow cover, groundwater, peatlands and rock glaciers. Additionally, snowmelt hotspots are good candidates for the installation of hydro-meteorological

stations, particularly in situations where only limited financial resources are available for the monitoring of large, remote regions. This study was carried out during a severe drought that affects the semiarid Andes since 2010. As current climate projections for this region suggest that droughts will be more frequent in the future, we expect that our results will be relevant in the context of climate change. In particular, they can be used to better understand the hydrological response of the semiarid Andes and to improve the planning and management of its water resources.

Acknowledgments

ÁA acknowledges ANID-Fondecyt postdoctoral project 3190732. We thank the project ANID-FONDEF IDeA I+D ID21I10129, ANID-CENTROS REGIONALES R20F0008 and all the people involved in the data collection on Tapado Glacier, particularly Ignacio Diaz. CEAZAmet is thanked for support with meteorological data acquisition. Gonzalo Cortés is kindly acknowledged for providing the SWE reconstruction dataset (Cortés and Margulis, 2017).

Data availability

Tapado and Paso Agua Negra meteorological data are freely available at www.ceazamet.cl. Tapado AWS appears in the webpage as El Tapado. Tapado Glacier meteorological data will be included in the same webpage.

Author contributions

ÁA designed the study with the collaboration of SM. ÁA led the collection at the Tapado Glacier field site. ÁA performed the SnowModel simulations and main analysis with the collaboration of SS. ÁA interpreted results and wrote the manuscript with the help of SM and SS.

Competing interests

The authors declare that they have no conflict of interest.

References

Alvarez-Garreton, C., Mendoza, P. A., Pablo Boisier, J., Addor, N., Galleguillos, M., Zambrano-Bigiarini, M., Lara, A., Puelma, C., Cortes, G., Garreaud, R., McPhee, J., Ayala, A., Álvarez-Garretón, C., Mendoza, P. A., Pablo Boisier, J., Addor, N., Galleguillos, M., Zambrano-Bigiarini, M., Lara, A., Puelma, C., Cortes, G., Garreaud, R., McPhee, J., and Ayala, A.: The CAMELS-CL dataset: Catchment attributes and meteorology for large sample studies-Chile dataset, Hydrol. Earth Syst. Sci., 22, 5817–5846, https://doi.org/10.5194/hess-22-5817-2018, 2018.

Alvarez-Garreton, C., Pablo Boisier, J., Garreaud, R., Seibert, J., and Vis, M.: Progressive water deficits during multiyear droughts in basins with long hydrological memory in Chile, Hydrol. Earth Syst. Sci., 25, 429–446, https://doi.org/10.5194/hess-25-429-2021, 2021.

Arias, P. A., Garreaud, R., Poveda, G., Espinoza, J. C., Molina-Carpio, J., Masiokas, M., Viale, M., Scaff, L., and van Oevelen, P. J.: Hydroclimate of the Andes Part II: Hydroclimate Variability and Sub-Continental Patterns, Front. Earth Sci., 8, 1–25, https://doi.org/10.3389/feart.2020.505467, 2021.

Ayala, A., Pellicciotti, F., Peleg, N., and Burlando, P.: Melt and surface sublimation across a glacier in a dry environment: Distributed energy-balance modelling of Juncal Norte Glacier, Chile, J. Glaciol., 63, 803–822, https://doi.org/10.1017/jog.2017.46, 2017a.

Ayala, A., Pellicciotti, F., MacDonell, S., McPhee, J., and Burlando, P.: Patterns of glacier ablation across North-Central Chile: Identifying the limits of empirical melt models under sublimation-favorable conditions, Water Resour. Res., 53, 5601–5625, https://doi.org/10.1002/2016WR020126, 2017b.

Ayala, Á., Farías-Barahona, D., Huss, M., Pellicciotti, F., McPhee, J., and Farinotti, D.: Glacier runoff variations since 1955 in the Maipo River basin, in the semiarid Andes of central Chile, Cryosph., 14, 2005–2027, https://doi.org/10.5194/tc-14-2005-2020, 2020.

Badger, A. M., Bjarke, N., Molotch, N. P., and Livneh, B.: The sensitivity of runoff generation to spatial snowpack uniformity in an alpine watershed: Green Lakes Valley, Niwot Ridge Long-Term Ecological Research station, Hydrol. Process., 35, 1–14, https://doi.org/10.1002/hyp.14331, 2021.

Brock, B. W., Willis, I. C., and Sharp, M. J.: Measurement and parameterization of aerodynamic roughness length variations at Haut Glacier d'Arolla, Switzerland, J. Glaciol., 52, 281–297, https://doi.org/10.3189/172756506781828746, 2006.

Cortés, G. and Margulis, S.: Impacts of El Niño and La Niña on interannual snow accumulation in the Andes: Results from a high-resolution 31 year reanalysis, Geophys. Res. Lett., 44, 6859–6867, https://doi.org/10.1002/2017GL073826, 2017.

Cortés, G., Girotto, M., and Margulis, S. a.: Snow process estimation over the extratropical Andes using a data assimilation framework integrating MERRA data and Landsat imagery, Water Resour. Res., 52, https://doi.org/10.1002/2014WR015716, 2016.

DeBeer, C. M. and Pomeroy, J. W.: Influence of snowpack and melt energy heterogeneity on snow cover depletion and snowmelt runoff simulation in a cold mountain environment, J. Hydrol., 553, 199–213, https://doi.org/10.1016/j.jhydrol.2017.07.051, 2017.

Información Oficial Hidrometeorológica y de Calidad de Aguas en Línea: https://snia.mop.gob.cl/BNAConsultas/reportes, last access: 20 January 2023.

DGA: Inventario Público de Glaciares, actualización 2022, 2022.

Dornes, P. F. P., Pomeroy, J. J. W., Pietroniro, A., Carey, S. K., and Quinton, W. L.: Influence of landscape aggregation in modelling snow-cover ablation and snowmelt runoff in a sub-arctic mountainous environment, Hydrol. Sci. J., 53, 725–740, https://doi.org/10.1623/hysj.53.4.725, 2008.

Level-2A Algorithm Overview: https://sentinels.copernicus.eu/web/sentinel/technical-guides/sentinel-2-msi/level-2a/algorithm, last access: 20 January 2023.

Favier, V., Falvey, M., Rabatel, A., Praderio, E., and Lopez, D.: Interpreting discrepancies between discharge and precipitation in high-altitude area of Chile's Norte Chico region (26-32°S), Water Resour. Res., 45, https://doi.org/10.1029/2008WR006802, 2009.

Freudiger, D., Kohn, I., Seibert, J., Stahl, K., and Weiler, M.: Snow redistribution for the hydrological modeling of alpine catchments, Wiley Interdiscip. Rev. Water, 4, e1232, https://doi.org/10.1002/wat2.1232, 2017.

Gascoin, S., Kinnard, C., Ponce, R., Lhermitte, S., MacDonell, S., and Rabatel, A.: Glacier contribution to streamflow in two headwaters of the Huasco River, Dry Andes of Chile, Cryosph., 5, 1099–1113, https://doi.org/10.5194/tc-5-1099-2011, 2011.

Gascoin, S., Lhermitte, S., Kinnard, C., Bortels, K., and Liston, G. E.: Wind effects on snow cover in Pascua-Lama, Dry Andes of Chile, Adv. Water Resour., 55, 25–39, https://doi.org/10.1016/j.advwatres.2012.11.013, 2013.

Ginot, P., Kull, C., Schotterer, U., Schwikowski, M., and Gäggeler, H. W.: Glacier mass balance reconstruction by sublimation induced enrichment of chemical species on Cerro Tapado (Chilean Andes), Clim. Past, 2, 21–30, https://doi.org/10.5194/cp-2-21-2006, 2006.

Groot Zwaaftink, C. D., Mott, R., and Lehning, M.: Seasonal simulation of drifting snow sublimation in Alpine terrain, Water Resour. Res., 49, 1581–1590, https://doi.org/10.1002/wrcr.20137, 2013.

Hock, R., Hutchings, J. K., and Lehning, M.: Grand Challenges in Cryospheric Sciences: Toward Better Predictability of Glaciers, Snow and Sea Ice, Front. Earth Sci., 5, 1–14, https://doi.org/10.3389/feart.2017.00064, 2017.

Hood, E., Williams, M., and Cline, D.: Sublimation from a seasonal snowpack at a continental, mid-latitude alpine site, Hydrol. Process., 1797, 1781–1797, 1999.

Huning, L. S. and AghaKouchak, A.: Global snow drought hot spots and characteristics, Proc. Natl. Acad. Sci. U. S. A., 117, 19753–19759, https://doi.org/10.1073/PNAS.1915921117, 2020.

Jackson, S. and Prowse, T.: Spatial variation of snowmelt and sublimation in a high-elevation semi-desert basin of western Canada, Hydrol. Process., 2627, 2611–2627, https://doi.org/10.1002/hyp, 2009.

Kalthoff, N., Fiebig-Wittmaack, M., Meißner, C., Kohler, M., Uriarte, M., Bischoff-Gauß, I., and Gonzales, E.: The energy balance, evapo-transpiration and nocturnal dew deposition of an arid valley in the Andes, J. Arid Environ., 65, 420–443, https://doi.org/10.1016/j.jaridenv.2005.08.013, 2006.

Kraaijenbrink, P. D. A., Stigter, E. E., Yao, T., and Immerzeel, W. W.: Climate change decisive for Asia's snow meltwater supply, Nat. Clim. Chang., 11, 591–597, https://doi.org/10.1038/s41558-021-01074-x, 2021.

Lehning, M., Bartelt, P., Brown, B., and Lehning, M.: A physical SNOWPACK model for the Swiss avalanche warning: Part II. Snow microstructure, Cold Reg. Sci. Technol., 35, 147–167, 2002.

Lehning, M., Löwe, H., Ryser, M., and Raderschall, N.: Inhomogeneous precipitation distribution and snow transport in steep terrain, Water Resour. Res., 44, W07404, https://doi.org/10.1029/2007WR006545, 2008.

Lhermitte, S., Abermann, J., and Kinnard, C.: Albedo over rough snow and ice surfaces, Cryosph., 8, 1069–1086,

https://doi.org/10.5194/tc-8-1069-2014, 2014.

Liston, G.: Local advection of momentum, heat, and moisture during the melt of patchy snow covers, J. Appl. Meteorol., 1995.

Liston, G., Sturm, M. H., En, G., Lr Ston, E., and Sturm, M. H.: A snow-transport model for complex terrain, J. Glaciol., 44, 498–516, https://doi.org/https://doi.org/10.3198/1998JoG44-148-498-516, 1998.

Liston, G. E. and Elder, K.: A distributed snow-evolution modeling system (snowmodel), J. Hydrometeorol., 7, 1259–1276, https://doi.org/10.1175/JHM548.1, 2006a.

Liston, G. E. and Hall, D. K.: An energy-balance model of lake-ice evolution, J. Glaciol., 41, 373–382, 1995.

Liston, G. E., Haehnel, R. B., Sturm, M., Hiemstra, C. A., Berezovskaya, S., and Tabler, R. D.: Simulating complex snow distributions in windy environments using SnowTran-3D, J. Glaciol., 53, 241–256, https://doi.org/10.3189/172756507782202865, 2007.

Liston, G. E. G. and Elder, K.: A meteorological distribution system for high-resolution terrestrial modeling (MicroMet), J. Hydrometeorol., 7, 217–234, https://doi.org/10.1175/JHM486.1., 2006b.

Litt, M., Shea, J., Wagnon, P., Steiner, J., Koch, I., Stigter, E., and Immerzeel, W.: Glacier ablation and temperature indexed melt models in the Nepalese Himalaya, Sci. Rep., 9, 1–13, https://doi.org/10.1038/s41598-019-41657-5, 2019.

Lliboutry, L.: The origin of penitents, J. Glaciol., 331–338, 1954.

Luce, C. H., Tarboton, D. G., and Cooley, K. R.: The influence of the spatial distribution of snow on basin-averaged snowmelt, Hydrol. Process., 12, 1671–1683, https://doi.org/10.1002/(SICI)1099-1085(199808/09)12:10/11<1671::AID-HYP688>3.0.CO;2-N, 1998.

MacDonell, S., Kinnard, C., Mölg, T., Nicholson, L., and Abermann, J.: Meteorological drivers of ablation processes on a cold glacier in the semi-arid Andes of Chile, Cryosph., 7, 1513–1526, https://doi.org/10.5194/tc-7-1513-2013, 2013.

Mankin, J. S., Viviroli, D., Singh, D., Hoekstra, A. Y., and Diffenbaugh, N. S.: The potential for snow to supply human water demand in the present and future, Environ. Res. Lett., 10, https://doi.org/10.1088/1748-9326/10/11/114016, 2015.

Masiokas, M. H., Villalba, R., Luckman, B. H., Le Quesne, C., and Aravena, J. C.: Snowpack variations in the central Andes of Argentina and Chile, 1951-2005: Large-scale atmospheric influences and implications for water resources in the region, J. Clim., 19, 6334–6352, https://doi.org/10.1175/JCLI3969.1, 2006.

Mendoza, P. A., Shaw, T. E., McPhee, J., Musselman, K. N., Revuelto, J., and MacDonell, S.: Spatial Distribution and Scaling Properties of Lidar-Derived Snow Depth in the Extratropical Andes, Water Resour. Res., 56, e2020WR028480, https://doi.org/https://doi.org/10.1029/2020WR028480, 2020.

Merkouriadi, I., Lemmetyinen, J., Liston, G. E., and Pulliainen, J.: Solving Challenges of Assimilating Microwave Remote Sensing Signatures With a Physical Model to Estimate Snow Water Equivalent, Water Resour. Res., 57, 1–24, https://doi.org/10.1029/2021WR030119, 2021.

Mernild, S. H., Liston, G. E., Hiemstra, C. A., Malmros, J. K., Yde, J. C., and McPhee, J.: The Andes Cordillera. Part I: snow distribution, properties, and trends (1979-2014), Int. J. Climatol., https://doi.org/10.1002/joc.4804, 2016.

Mernild, S. H., Liston, G. E., Hiemstra, C. A., Yde, J. C., and Casassa, G.: Annual river runoff variations and trends for the

Andes Cordillera, J. Hydrometeorol., 19, 1167–1189, https://doi.org/10.1175/JHM-D-17-0094.1, 2018.

Montecinos, A. and Aceituno, P.: Seasonality of the ENSO-related rainfall variability in central Chile and associated circulation anomalies, J. Clim., 16, 281–296, https://doi.org/10.1175/1520-0442(2003)016<0281:SOTERR>2.0.CO;2, 2003.

Mott, R., Schirmer, M., Bavay, M., Grünewald, T., and Lehning, M.: Understanding snow-transport processes shaping the mountain snow-cover, Cryosph., 4, 545–559, https://doi.org/10.5194/tc-4-545-2010, 2010.

Mott, R., Vionnet, V., and Grünewald, T.: The Seasonal Snow Cover Dynamics: Review on Wind-Driven Coupling Processes, Front. Earth Sci., 6, https://doi.org/10.3389/feart.2018.00197, 2018.

Mott, R., Stiperski, I., and Nicholson, L.: Spatio-temporal flow variations driving heat exchange processes at a mountain glacier, Cryosph., 14, 4699–4718, https://doi.org/10.5194/tc-14-4699-2020, 2020.

NASA JPL: NASADEM Merged DEM Global 1 arc second V001 [Data set], https://doi.org/10.5067/MEaSUREs/NASADEM/NASADEM_HGT.001, 2020.

Nicholson, L. I., Petlicki, M., Partan, B., and Macdonell, S.: 3D surface properties of glacier penitentes over an ablation season, measured using a Microsoft Xbox Kinect, Cryosph., 10, 1897–1913, https://doi.org/10.5194/tc-2015-207, 2016.

Palm, S. P., Kayetha, V., Yang, Y., and Pauly, R.: Blowing snow sublimation and transport over Antarctica from 11 years of CALIPSO observations, Cryosph., 11, 2555–2569, https://doi.org/10.5194/tc-11-2555-2017, 2017.

Pitte, P., Masiokas, M., Gargantini, H., Ruiz, L., Berthier, E., Ferri Hidalgo, L., Zalazar, L., Dussaillant, I., Viale, M., Zorzut, V., Corvalán, E., Scarpa, J. P., Costa, G., and Villalba, R.: Recent mass-balance changes of Agua Negra glacier (30°S) in the Desert Andes of Argentina, J. Glaciol., 1–13, https://doi.org/10.1017/jog.2022.22, 2022.

Pomeroy, J. J. W., Toth, B., Granger, R. J. J., Hedstrom, N. R. R., and Essery, R. L. H. L. H.: Variation in surface energetics during snowmelt in a subarctic mountain catchment, J. Hydrometeorol., 4, 702–719, https://doi.org/10.1175/1525-7541(2003)004<0702:VISEDS>2.0.CO;2, 2003.

Pomeroy, J. W. and Li, L.: Prairie and arctic areal snow cover mass balance using a blowing snow model, J. Geophys. Res., 105, 26619, https://doi.org/10.1029/2000JD900149, 2000.

Pomeroy, J. W., Gray, D. M., Shook, K. R., Toth, B., Essery, R. L. H., Pietroniro, A., and Hedstrom, N.: An evaluation of snow accumulation and ablation processes for land surface modelling, Hydrol. Process., 12, 2339–2367, https://doi.org/https://doi.org/10.1002/(SICI)1099-1085(199812)12:15<2339::AID-HYP800>3.0.CO;2-L, 1998.

Pourrier, J., Jourde, H., Kinnard, C., Gascoin, S., and Monnier, S.: Glacier meltwater flow paths and storage in a geomorphologically complex glacial foreland: The case of the Tapado glacier, dry Andes of Chile (30°S), J. Hydrol., 519, 1068–1083, https://doi.org/10.1016/j.jhydrol.2014.08.023, 2014.

Ragettli, S., Cortés, G., Mcphee, J., and Pellicciotti, F.: An evaluation of approaches for modelling hydrological processes in high-elevation, glacierized Andean watersheds, Hydrol. Process., 28, 5674–5695, https://doi.org/10.1002/hyp.10055, 2014.

Réveillet, M., MacDonell, S., Gascoin, S., Kinnard, C., Lhermitte, S., and Schaffer, N.: Impact of forcing on sublimation simulations for a high mountain catchment in the semiarid Andes, Cryosph., 14, 147–163, https://doi.org/10.5194/tc-14-147-2020, 2020.

https://doi.org/10.5194/hess-2023-23
Preprint. Discussion started: 31 January 2023


Hydrology and Earth System Sciences
Discussions

Robson, B. A., MacDonell, S., Ayala, Á., Bolch, T., Nielsen, P. R., and Vivero, S.: Glacier and Rock Glacier changes since the 1950s in the La Laguna catchment, Chile, Cryosph., 16, 647–665, https://doi.org/10.5194/tc-2021-200, 2022.

Rodriguez, M., Ohlanders, N., Pellicciotti, F., Williams, M. W., and Mcphee, J.: Estimating runoff from a glacierized catchment using natural tracers in the semi-arid Andes cordillera, Hydrol. Process., 30, 3609–3626, https://doi.org/10.1002/hyp.10973, 2016.

Saavedra, F., Cortés, G., Viale, M., Margulis, S., and McPhee, J.: Atmospheric Rivers Contribution to the Snow Accumulation Over the Southern Andes (26.5° S–37.5° S), Front. Earth Sci., 8, 1–11, https://doi.org/10.3389/feart.2020.00261, 2020.

Sarricolea, P., Herrera-Ossandon, M., and Meseguer-Ruiz, Ó.: Climatic regionalisation of continental Chile, J. Maps, 13, 66–73, https://doi.org/10.1080/17445647.2016.1259592, 2017.

Scaff, L., Rutllant, J. A., Rahn, D., Gascoin, S., and Rondanelli, R.: Meteorological Interpretation of Orographic Precipitation Gradients along an Andes West Slope Basin at 30°S (Elqui Valley, Chile), J. Hydrometeorol., 18, 713–727, https://doi.org/10.1175/JHM-D-16-0073.1, 2017.

Schaffer, N., MacDonell, S., Réveillet, M., Yáñez, E., and Valois, R.: Rock glaciers as a water resource in a changing climate in the semiarid Chilean Andes, Reg. Environ. Chang., 2, https://doi.org/10.1007/s10113-018-01459-3, 2019.

Schauwecker, S., Palma, G., MacDonell, S., Ayala, Á., and Viale, M.: The Snowline and 0°C Isotherm Altitudes During Precipitation Events in the Dry Subtropical Chilean Andes as Seen by Citizen Science, Surface Stations, and ERA5 Reanalysis Data, Front. Earth Sci., 10, 1–19, https://doi.org/10.3389/feart.2022.875795, 2022.

Seibert, J., Vis, M. J. P., Kohn, I., Weiler, M., and Stahl, K.: Technical Note: Representing glacier dynamics in a semi-distributed hydrological model, Hydrol. Earth Syst. Sci. Discuss., 1–20, https://doi.org/10.5194/hess-2017-158, 2017.

Sinclair, K. E. and MacDonell, S.: Seasonal evolution of penitente glaciochemistry at Tapado Glacier, Northern Chile, Hydrol. Process., 30, n/a-n/a, https://doi.org/10.1002/hyp.10531, 2015.

Sproles, E. A., Kerr, T., Orrego Nelson, C., and Lopez Aspe, D.: Developing a Snowmelt Forecast Model in the Absence of Field Data, Water Resour. Manag., 30, 2581–2590, https://doi.org/10.1007/s11269-016-1271-4, 2016.

Stigter, E. E., Litt, M., Steiner, J. F., Bonekamp, P. N. J., Shea, J. M., Bierkens, M. F. P., and Immerzeel, W. W.: The Importance of Snow Sublimation on a Himalayan Glacier, Front. Earth Sci., 6, 1–16, https://doi.org/10.3389/feart.2018.00108, 2018.

Strasser, U., Bernhardt, M., Weber, M., Liston, G. E., and Mauser, W.: Is snow sublimation important in the alpine water balance?, Cryosph., 2, 53–66, 2008.

van der Valk, L. D., Teuling, A. J., Girod, L., Pirk, N., Stoffer, R., and van Heerwaarden, C. C.: Understanding wind-driven melt of patchy snow cover, Cryosph., 16, 4319–4341, https://doi.org/10.5194/tc-16-4319-2022, 2022.

Valois, R., Schaffer, N., Figueroa, R., Maldonado, A., Yáñez, E., Hevia, A., Carrizo, G. Y., and MacDonell, S.: Characterizing the water storage capacity and hydrological role of mountain peatlands in the arid andes of North-Central Chile, Water (Switzerland), 12, https://doi.org/10.3390/W12041071, 2020.

Vionnet, V., Brun, E., Morin, S., Boone, A., Faroux, S., Le Moigne, P., Martin, E., and Willemet, J.-M. M.: The detailed

snowpack scheme Crocus and its implementation in SURFEX v7.2, Geosci. Model Dev., 5, 773–791, https://doi.org/10.5194/gmd-5-773-2012, 2012.

Voordendag, A., Réveillet, M., MacDonell, S., and Lhermitte, S.: Snow model comparison to simulate snow depth evolution and sublimation at point scale in the semi-arid Andes of Chile, Cryosph., 15, 4241–4259, https://doi.org/10.5194/tc-15-4241-2021, 2021.

Wayand, N. E., Marsh, C. B., Shea, J. M., and Pomeroy, J. W.: Globally scalable alpine snow metrics, Remote Sens. Environ., 213, 61–72, https://doi.org/10.1016/j.rse.2018.05.012, 2018.

Zhang, Y. and Ishikawa, M.: Sublimation from thin snow cover at the edge of the Eurasian cryosphere in Mongolia, Hydrol. Process., 3575, 3564–3575, https://doi.org/10.1002/hyp, 2008.